Université du Québec
Institut National de la Recherche Scientifique
Center for Energy Materials and Telecommunications

Development of an antiviral, compostable filtration material for use in surgical face masks

By

Eve Lambert-Fliszar

A thesis submitted to the Department of Energy, Materials and Telecommunications in conformity with the requirements for the degree of Master of Science (M.Sc.)

Submitted on December 17, 2021

Evaluation Jury

President of the jury Internal examiner	Prof. Fiorenzo Vetrone INRS-EMT, Université du Québec
External examiner	Prof. Louis Cuccia Department of Chemistry & Biochemistry Concordia University
Research Director	Prof. Federico Rosei INRS-EMT, Université du Québec

ACKNOWLEDGEMENTS

I would first like to thank my supervisor, Professor Federico Rosei, as well as Sumitra Rajagopalan for giving me the opportunity to work on this project. Conducting research in tandem with industry experience has given me product development skills in addition to allowing me to form the ability to conduct fundamental research. I would also like to thank Dr. Daniele Benetti for his guidance and encouragement throughout the last year; I have learned tremendously from our discussions, and appreciate the time he took to provide advice and feedback. Finally, I'd like to extend my appreciation to my friend and colleague Elena Lombardo, with whom I had the chance to collaborate throughout this process. This experience would not have been the same without the invaluable knowledge and positive attitude she has shared with me.

In addition to the team at INRS-EMT, I would like to thank my colleagues at Bioastra Technologies Inc: Jean-Richard Bullet, Prajwal Kumar, Robert Poulin, Jamila Cissé, and Oscar Suarez. The generosity with which they shared their time and knowledge has allowed me to grow tremendously as a researcher.

Finally, I would like to thank Professor Laurent Chatel-Chaix and his team from the Armand-Frappier Santé Biotechnologie Research Centre. Their expertise allowed me to gain valuable knowledge in an area I was previously unfamiliar with; without their contributions, the viral component of this work would not have been possible.

ABSTRACT

The COVID-19 pandemic has increased awareness of the importance of personal protective equipment (PPE) in the prevention of viral transmission. The waste associated with PPE, however, has alerted the public to the worsening pollution crisis. Current surgical masks commonly used are comprised of nonwoven polypropylene fabric, which is derived from petroleum, a non-renewable resource. Furthermore, the disposal of these masks has resulted in significant waste. In this work, I present the development of an improved surgical mask that considers the needs of a growing population and a changing climate, both factors which may increase the prevalence of disease. To this end, a compostable, bio-based, and antiviral filtration material is developed which can be used to prepare masks to enhance user protection from virus transmission while limiting the waste associated with PPE.

This work aims to (i) create an inexpensive nonwoven compostable filtration material having comparable filtration and air flow properties to existing surgical masks and (ii) functionalize this material using a cationic polymer to inactivate viruses. Poly(lactic acid) is used as the base polymer for the nonwoven fibers since it is commercially available, relatively inexpensive, and biodegradable. Chitosan, another biodegradable polymer, is used to impart charge on the material in order to interact with and potentially inactivate viruses that land on the surface. The morphology and structure of the microfibers are characterized. Additionally, the filtration and breathability of the filter membrane are measured and compared to the current surgical masks filter. Finally, the antiviral activity of the filter material is studied against HCoV-OC43, the virus causing the common cold which has a similar configuration to the SARS-CoV-2 virus.

KEYWORDS: biodegradable; compostable; fibers; surgical mask; antiviral

RÉSUMÉ

La pandémie de COVID-19 a montré au public l'importance des équipements de protection individuelle (EPI) dans la prévention de la transmission du virus. Cependant, les déchets associés aux EPI ont alerté le public de la pollution qu'ils causent. Les masques chirurgicaux présentement utilisés sont constitués de tissu de polypropylène non tissé, qui est dérivé d' une ressource non-renouvelable – le pétrole. De plus, ces masques sont utilisés qu'une seule fois, ce qui entraine un gaspillage important. Dans ce mémoire, je discute le développement d'un masque chirurgical amélioré qui tient compte des besoins d'une population croissante et d'un climat changeant, deux facteurs qui peuvent augmenter la prévalence de la maladie. À cette fin, un matériau de filtration compostable et antiviral est développé qui peut être utilisé pour préparer des masques afin d'améliorer la protection des utilisateurs contre la transmission de virus tout en limitant les déchets associés aux EPI.

Ce travail vise à (i) créer un matériau de filtration compostable non-tissé peu coûteux ayant des propriétés de filtration et de circulation d'air comparables aux masques chirurgicaux existants et (ii) fonctionnaliser ce matériau à l'aide d'un polymère cationique pour inactiver les virus. Le poly(acide lactique) est utilisé comme polymère de base pour former les fibres non-tissées car il est relativement peu coûteux et biodégradable. Le chitosane, un autre polymère biodégradable, est utilisé pour accorder une charge au matériau afin d'interagir avec et potentiellement inactiver les virus qui atterrissent sur la surface. La morphologie et la structure des microfibres sont caractérisées. De plus, la filtration et la résistance à l'air de la membrane filtrante sont mesurées et comparées au filtre actuel des masques chirurgicaux. Enfin, l'activité antivirale du matériau filtrant est étudiée contre HCoV-OC43, le virus à l'origine du rhume qui a une configuration similaire au virus SARS-CoV-2.

MOTS CLÉS: biodegradable; compostable; fibres, masque chirurgical; antiviral

TABLE OF CONTENTS

TABLE OF TABLES

TABLE OF FIGURES

TABLE OF EQUATIONS

TABLE OF ABBREVIATIONS

A…….. .....Cross-sectional surface area

A_0…….....Reference absorption

A_1…….....Sample Absorption

ACE2…. .....Angiotensin-converting enzyme type 2

ASTM…… .....American Society for Testing and Materials

BET…..... …. Brunauer-Emmett-Teller

BJH…… ..... . Barrett-Joyner-Halenda

COVID-19……..Coronavirus disease 2019

CS…..... Chitosan

DCM……Dichloromethane

DMEM……..…… Dulbecco's Modified Eagle Medium

DSC… ..... Differential scanning calorimetry

FTIR .....… Fourier-transform infrared

H_o….....Standard enthalpy of melting

H_s….....Enthalpy of melting

LB……..….Luria Broth

M…..... Molecular weight

N… ..... Avogadro's number

PBS……..……..……..……..……..……..……..Phosphate buffer solution

PEI…..Polyethylenimine

PLA.. .....Poly(lactic acid)

PP…..Polypropylene

PPE……..…Personal protective equipment

RNA…. .....Ribonucleic acid

SEM…..Scanning electron microscope

T_g… .....Glass transition temperature

T_m….. .....Metling temperature

UV-vis…. .....Ultraviolet-visible

W_s…..Sample weight

XRD…..X-ray powder diffraction

ε_r…..Dielectric constant

1 INTRODUCTION

Throughout the COVID-19 pandemic facemasks have proven to be effective in diminishing transmission of this respiratory virus. These will surely remain the first line of defense in the next outbreak of a respiratory illness. As the world slowed to a stop during the pandemic, it became clear to many that the scale of this pandemic and our relationship with the planet and its resources are heavily intertwined. Studies show that the depletion of natural habitats has brought humans closer than ever before to animals which carry pathogens previously unknown to us. Thus, some predict that humanity will see an increase in the transmission of diseases from animals to humans [1]. Furthermore, amid the chaos of the pandemic, people around the world have experienced record-breaking wildfire, flooding, and hurricane seasons. It is clear that the pandemic is not the only life-threatening danger humanity faces – climate change and the collapse of ecosystems have and will continue to introduce threats to humans.

Our global economy currently has a linear supply chain for most of the products we use; raw materials are extracted from the ground, processed into a product, which is then consumed and finally thrown in a landfill. Implementing principles of a circular economy would greatly reduce this waste, rather than continuously take raw materials from the earth and place them in a landfill once the product is used. In this economy model, resources are continuously recycled and reused, thereby minimizing the raw material extraction from the earth as well as reducing waste. During the pandemic, people all over the world have become well acquainted with the surgical mask, as it has proven to be a great tool in minimizing the spread of COVID-19. Unfortunately, the lifecycle of these masks typically follows a linear model. In 2020, 52 billion plastic facemasks were produced; the raw materials for these were obtained by drilling fossil fuels from the earth [2]. These masks, which are rarely recycled, nearly all ended up in landfills or littering our communities [3]. To address the issues of resource depletion and the transmission of this deadly virus, the idea was born to develop a product which can help address both; improve our ability to tackle the pandemic while keeping the planet in mind during product development. This work discusses the development of an antiviral and compostable face

mask which can not only protect humankind from airborne diseases, but does so while implementing principles of a circular economy. No longer should humans take from the earth only to throw its resources in a landfill; rather, we should be returning Earth's resources to the ground and reuse these resources indefinitely.

1.1 Masks

Face masks have been an integral part in the worldwide public health strategy for mitigation of the COVID-19 pandemic. Respiratory illnesses, such as COVID-19, can spread through the air as infected persons breathe or speak, releasing virus-containing aerosols into the air which are then inhaled by others nearby. Masks, therefore, act as the first barrier between an infected person and the outside world, while also protecting non-infected people from inhaling the virus.

1.1.1 General mask design

Surgical masks typically consist of three plies of polypropylene (PP) fabric. Elastic ear loops hold the mask to the user's face, while a metal or plastic nose bridge fits the mask more closely to the skin, minimizing air flow through gaps between the skin and the mask.

There are three layers in a surgical mask; the two exterior layers consist of spunbond PP fabric. The spunbond process, in which molten polymer is spun while stretched, produces large fibers. These layers' principal role is to provide mechanical structure to the mask so that it can be manipulated without tearing. Furthermore, the spunbond polymer results in a more comfortable material to wear against the skin. Due to the large fiber size, it does not provide much filtration, however. Between these two spunbond layers is a filtration layer, which is the focus of the work described in this thesis as it is more technologically involved as well as being more important than the exterior layers in providing protection. Typically, this middle layer is made via meltblowing, which results in a mat of nonwoven fibers smaller than the fibers of the exterior layer.

The primary mechanism upon which face masks rely is basic filtration; the fibers which make up the mask physically block airborne particles from passing through the material.

Advanced masks, however, such as surgical masks and respirators, rely on an additional mechanism – electrostatic entrapment of these particles [5]. This work discusses the development of a surgical mask – an inexpensive, widely-used mask that combines both physical and electrostatic mechanisms.

1.1.2 Surgical mask specifications

Because this work aims to develop a mask which can replace polypropylene surgical masks on the market, it is critical that the mask meets certain specifications for surgical masks. Table 1 below is from the American Society for Testing and Materials (ASTM) standard which governs surgical mask specifications; it outlines the standards required for a face mask to be considered a "medical," or surgical face mask. The work described herein studies the following characteristics from the ASTM standard: filtration and breathability (differential pressure). Owing to equipment limitations, the experiments performed for this thesis do not follow strictly the protocol outlined by the ASTM standard. Therefore, instead of comparing results entirely to the requirements outlined in Table 1, the results of the experiments performed on the prepared filters are compared to a commercially available surgical mask filter as a benchmark.

Table 1. Medical face mask material requirements by performance level [6].

Characteristic	Level 1 Barrier	Level 2 Barrier	Level 3 Barrier
Bacterial filtration efficiency, %	≥95	≥98	≥98
Differential pressure, mm H_2O/cm^2	<5.0	<6.0	<6.0
Sub-micron particulate filtration efficiency at 0.1 micron, %	≥95	≥98	≥98
Resistance to penetration by synthetic blood, minimum pressure in mm Hg for pass result	80	120	120
Flame spread	Class 1	Class 1	Class 1

In order to meet the above requirements, the surgical mask must possess certain characteristics. First, it must be sufficiently porous to allow air to flow comfortably across the filter. Conversely, however, its fibers must be sufficiently packed in order to prevent

the passage of airborne molecules through the filter. Additionally, the filter should be hydrophobic to prevent the ingress of aerosols through the filter, as this could contribute to the penetration of pathogenic particles through the mask. The hydrophobicity of the filter surface may also prevent microbial adhesion, enhancing user protection [7]. Additional requirements for the filter developed here include compostability of the filter as well as antiviral activity of the surface.

1.1.3 Filtration mechanisms

One of the challenges in designing a high-efficiency mask is achieving high filtration efficiency of particles of various sizes, since particles with different masses behave differently. The largest particles (i.e.larger than 1 μm) are filtered in an intuitive manner; as they travel through the air, they are too large to pass between the fibers of the filter, thus preventing them from penetrating the mask [8]. The large particles adhere to the fibers of the mask via van der Waals forces.

The smallest particles (less than 0.2 μm in diameter) behave much differently. Even though they are small enough to pass between the fibers of the mask, their low mass means they collide with molecules in the air. Due to their Brownian motion, they are statistically likely to collide with a fiber of the mask [8]. These particles also adhere to the fibers of the mask via Waals forces.

Particles between 0.2 and 0.6 μm are too heavy to exhibit Brownian motion, yet too light for their inertia to result in a collision with fibers. As a result, these medium particles are entrained in the air which flows in and out of the mask and cannot be filtered mechanically. To prevent the penetration of these particles through the mask, electrostatic filtration is employed, typically via corona discharge treatment. In this process, the filtration material is placed in a high voltage electric field for a short period of time, thereby charging the material. By applying an electrostatic charge to the filtration material, traveling aerosols, which are charged due to interactions with the air, are attracted and adhere to the fibers. Charging a filter can improve its filtration by 21– 49%, depending on the density of the filter [8][5][9].

In a typical mask assembly line, filters are charged via corona discharge treatment. A voltage on the order of 10s of kV is applied for approximately one minute, resulting in the formation of an electric field between the point electrode and the plate electrode where the filter lies. As the electric field is very intense, it ionizes atoms in the air which create a chain reaction of ionization which eventually reaches the mask [10]. Since meltblown polypropylene exhibits a semi-crystalline structure, charges a stored in the crystallites [11]. These charges become trapped in the polymer structure. Temperature and humidity can diminish the charge density of the filter as they can loosely bound charges. Thus, these crystallites are imperative in retaining charge in a multitude of use conditions. Especially important in the context of masks is the degree of humidity; because exhaled breath contains a high amount of water molecules, loose charges are at risk of neutralization.

1.2 **Antiviral Mechanism**

The SARS-CoV-2 virus is an enveloped coronavirus, meaning its RNA is contained inside a lipid-bilayer membrane, similar to that which encases living cells. It has an outer diameter of 91 ± 11 nm, measured around the circumference of the spikes that form its characteristic “corona,” or crown. These spikes are positively charged along the top of the protein, which allows to the virus to bind to and infect host cells [12] [13]. The spike glycoproteins, however, are not uniformly charged; they have a net negative charge over the middle and lower parts of the spike [14]. The lipid membrane of the virus is also positive [15].

Viruses infect host cells by binding to them, then inserting their RNA into the living cell, and using the cell’s replication mechanisms to replicate the viral RNA. When the virus’ membrane is broken, however, its RNA leaks out of the virus, rendering it inactive [16]. In general, it is believed that polycations adhere to lipid bilayer membranes and induce segregation or transmembrane migration of lipid molecules, resulting in a leakage of the viral RNA [17]. This is the targeted mechanism for antiviral activity; it is summarized in Figure 1 below [18].

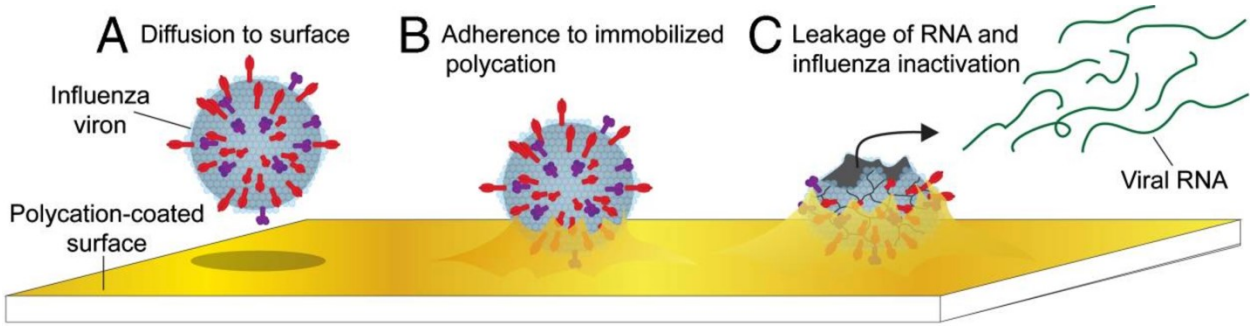

Figure 1. **Proposed antiviral mechanism resulting in membrane disruption and viral RNA leakage [18].**

Hsu et al. have previously demonstrated the antiviral behavior of cationic polymers against the influenza virus. Like SARS-CoV-2 and pathogenic bacteria, the influenza virus is also enveloped by a lipid membrane [19]. In his work, N,N-Dodecyl,methyl-polyethylenimine (PEI), a polycationic polymer, demonstrates a 10,000-fold reduction in viral infectivity within minutes of contact with the influenza virus suspended in a PBS solution [16]. Further studies of this antiviral mechanism confirm that the polycationic nature of the polymer was responsible for disruption of the membrane, as was confirmed by SEM, shown in Figure 2 below [18].

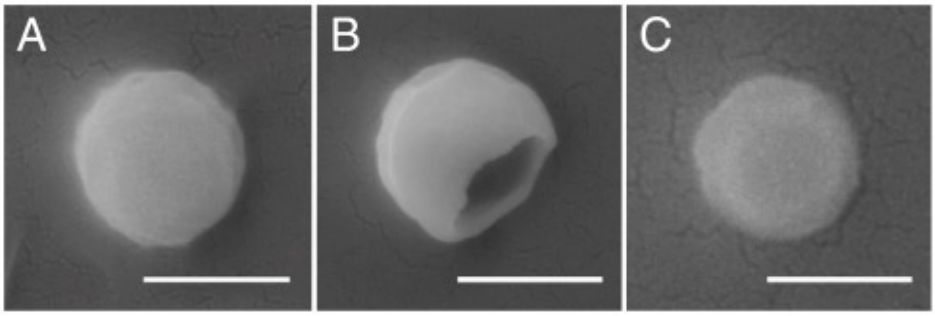

Figure 2. **SEM image of influenza virus on uncoated silicon wafer (A) and N,N-Dodecyl,methyl-PEI coated silicon wafer (B and C). The majority of viruses demonstrated a disrupted membrane (B) while some remained intact (C). Scale bars represent 100 nm [18].**

Other polycationic polymers have been studied to assess their antiviral activity. In this work, chitosan, a known antimicrobial biopolymer is studied. Studies have been undertaken to assess the antibacterial effect of chitosan's cationic charge. By the same logic used by Hsu et. al, the antibacterial properties in chitosan may translate to antiviral properties in enveloped viruses.

Another antiviral mechanism proposed by Milewska et al. involves the inactivation of a virus by inhibiting it from infecting the host cell. In this work, modified chitosan (HTCC) was shown to prevent the binding of the HCoV-NL63 virus to the cellular receptor, angiotensin-converting enzyme type 2 (ACE2) protein via confocal microscopy. The ACE2 is a common receptor, especially in lung epithelial cells, which is why SARS-CoV-2 poses a particular threat to respiratory airways [20]. Thus, while the virus remains intact, it is unable to infect the human cell for replication [21].

1.2.1 Chitosan

Chitosan is a biopolymer derived from the deacetylation of chitin, which can be readily obtained from the shells of crustaceans. Its structure can be seen in Figure 3 below [22]. Due to its biocompatibility, low toxicity, antibacterial activity and biodegradability, it is often used in the biopharmaceutical industry, such as for drug delivery [22]. At a pH below 6.5, the amine groups ionize, imparting a cationic charge to the polymer as well as allowing it to dissolve in acidic mediums.

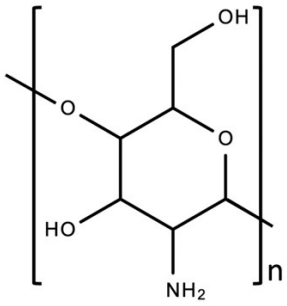

Figure 3. Molecular structure of chitosan.

The proposed mechanism herein relies on the cationic charge of chitosan to inactivate the virus. Because the water molecules in exhaled breath have a slightly acidic pH, aerosol droplets exhaled from an infected individual can result in the local ionization of chitosan molecules on the mask [23]. The charged amine groups may then come into contact with any viruses suspended in this droplet, thereby interfering with their envelope and rendering them inactive. It has been suggested that a higher molecular weight chitosan would have a greater antiviral effect due to the long chain length being able to penetrate between the spikes on the surface of a coronavirus, directly interacting with the

envelope membrane [24] [25].

1.3 **Poly(lactic acid)**

Poly(lactic acid) (PLA), shown in Figure 4 below, is used in this work to form the nonwoven fibers. It is a thermoplastic polyester made from the ring-opening polymerization of lactide. It can be derived from plant material, such as corn or sugarcane, making it a renewable polymer [26]. PLA has similar mechanical properties to PP, making it a suitable biodegradable replacement in facemasks. Furthermore, like PP, it is an electret material and can therefore be charged electrostatically [9]. Notably, PLA is the most widely used and least expensive biopolymer on the market and can be procured relatively easily. Thus, from a commercialization perspective, this is an ideal polymer as it is already commercially available at a cost similar to that of polypropylene.

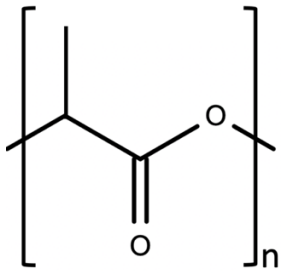

Figure 4. Molecular structure of PLA.

Furthermore, PLA is a biodegradable polymer. Its biodegradation mechanisms can be divided into two key steps: hydrolysis and microbial degradation. When composted, PLA can completely decompose into carbon, water, and carbon dioxide. Composting involves the use of a controlled environment for the degradation of organic material. Moisture content, acidity, temperature, and oxygen content of the mix is carefully monitored to optimize degradation conditions. In the first step of PLA degradation, water molecules permeate the polymer structure and cleave ester bonds, forming oligomers and eventually lactic acid. Since water molecules can more easily permeate the polymer in amorphous regions, highly crystalline PLA degrades slower than a more amorphous PLA. Next, microbes in the compost medium consume the oligomers and lactic acid monomers and convert them into carbon dioxide [27].

1.4 Thesis objectives and contributions

In this work, the main aim is to develop a filtration material made of compostable biopolymers that can compete with the filtration layer of traditional surgical masks. To do so, a PLA filter is prepared using an inexpensive and accessible method. The filter is then coated with chitosan to provide a potential antiviral effect. The objectives of this work are as follows:

1) Produce PLA fibers via spray pyrolysis method, apply chitosan coating, and characterize the fiber morphology and structure.
2) Assess the filtration performance of the fibers as a filtration material.
3) Investigate the compostability of the filter in a time-effective manner.
4) Study the antiviral properties imparted by the chitosan coating against HCoV-OC43, the virus responsible for influenza.

These objectives must be met while keeping product commercialization in mind; as such, the materials and methods must be inexpensive and industrially viable.

1.5 Thesis organisation

This thesis is organized in the following manner:

Section 1 outlines and introduces the purpose of this work.

Section 2 describes the experimental methodology used to synthesize and characterize the fibers and the resulting filters.

Section 3 provides the results of the experiments performed and discusses the significance of the results.

Section 4 discusses potential applications of bio-based compostable filters and antiviral coatings.

Section 5 summarizes the work and discusses future prospects of biobased compostable face masks.

2 MATERIALS AND METHODS

This chapter discusses the preparation of the fibrous filter material using spray pyrolysis. First, a PLA solution is sprayed onto a bath of water to create a randomly oriented mat of fibers. Chitosan is then coated onto the fiber mat to impart antiviral properties. The characterization conducted in this work is two-fold; first, the fibers are characterized on a microscopic scale to understand their morphology and properties. Then, the overall filter performance is characterized to assess its potential in real-life use as a surgical mask filtration layer.

2.1 Materials

PLA pellets used for this research were L-105 grade PLA resin from Total Corbion PLA (Gorinchem, Holland). This grade is specially produced for optimal performance in fiber-forming processes. Medium molecular weight chitosan (degree of deacetylation = 75-85%) was obtained from MilliporeSigma (Burlington, MA, USA). Dichloromethane and acetic acid were obtained from Fisher Scientific (Hampton, NH, USA). All chemicals were used as received.

2.2 Methods

2.2.1 PLA filter preparation

First, PLA was dissolved in dichloromethane (8 wt%) by stirring for two hours until the solution was clear. Dichloromethane (DCM) was used due to its ability to readily dissolve this grade of PLA, in addition to having a low vaporization point of 40 °C. This allows for the solvent to vaporize in the time it takes for the polymer solution to reach the water bath, leaving behind only fibers instead of casting a PLA film. DCM, however, is rather toxic and therefore not ideal to use on an industrial scale. Other solvents which are more industrially viable, such as acetone and ethyl acetate, were evaluated. These solvents, however, were not able to dissolve this grade of PLA and are therefore not suitable for this work. For future considerations, a more eco-friendly product could be developed by

assessing various grades of PLA. Here, only one sample could be obtained in sufficient quantity for this work; the L-105 grade was selected because it is formulated in a way that allows it to form fibers. This grade has the disadvantage, however, of being insoluble in industrially accepted solvents such as acetone and ethyl acetate. With more time and financial resources, other grades of PLA would have been assessed in order to find one which can dissolve in these solvents.

The prepared PLA solution was then sprayed using an airbrush obtained from Badger Air-Brush Co. (Franklin Park, IL, USA) at a distance of 25 cm from the surface of the room-temperature water bath using a pressure of 0.2 MPa. As the jet of polymer solution traveled to the surface of the water, the solvent vaporized leaving behind PLA microfibers. The polymer was sprayed in a raster pattern in order to cover the desired area. The setup for the spray pyrolysis process is shown in Figure 5 below.

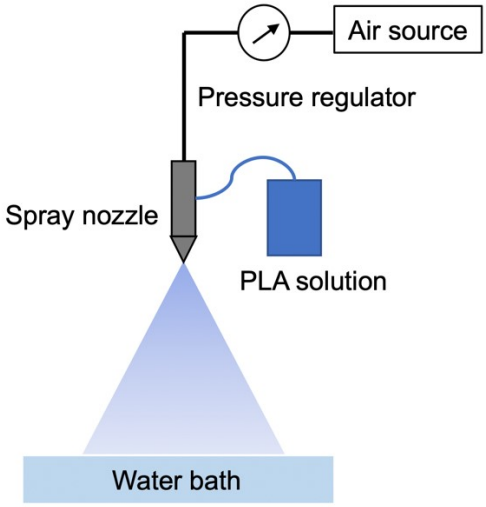

Figure 5. Setup for PLA filter pro duction via spray pyrolysis.

Due to the hydrophobicity of the PLA, the fibers formed a mat which floated above the water. Once the desired thickness was achieved, the filter was then lifted from the water using a frame, as shown in Figure 6 below. The mat was then dried in an oven at 60 °C for 10 minutes to evaporate any remaining water and finally removed from the frame.

Figure 6. PLA filter after removal from water bath.

It should be noted that this method was developed as a simple and inexpensive way to produce fibers, since meltblowing equipment constitutes a large investment and was not readily available during the pandemic. For commercializing this filter into a final product, the use of meltblowing as a fiber-forming technique would be preferred as it would simplify the adoption of this product into existing assembly line. This spray pyrolysis method, however, is a valuable alternative for lab-scale prototyping.

2.2.2 Chitosan coating

For the antiviral coating, a chitosan solution was prepared by dissolving chitosan in a 0.2% (v/v) solution of acetic acid. Two concentrations were used: a 0.2 wt% chitosan solution and 0.8 wt% (in weight of acetic acid solution), hereby referred to as PLA/CS1 and PLA/CS2, respectively.

The prepared PLA filter was then dipped in one of the chitosan solutions for 2 minutes, then rinsed three times in distilled water for 30 seconds per rinsing cycle. The filters were then dried in an oven at 60 °C for 10 minutes to evaporate any remaining water.

2.1 Characterization Techniques

2.1.1 Filtration

The filtration test used in this study was adapted from ASTM 2101-19: Standard Test Method for Evaluating the Bacterial Filtration Efficiency (BFE) of Medical Face Mask Materials, Using a Biological Aerosol of Staphylococcus aureus. In this test, a solution containing bacteria is nebulized and directed towards the filter as a test material. On the other side of the filter is an agar plate, which is collected once the test is complete after 2 minutes. The test is run again with no filter in place as a positive control. The two agar plates are incubated and the difference in bacterial growth is correlated to filtration efficiency [28].

Owing to the difficulties to access to a lab equipped for handling bacteria, the test used herein only assesses the aerosol permeability of the mask instead of bacterial permeability. Rather than a bacterial solution, methylene blue dye is used to dye aerosolized water. The quantity of dyed aerosols passing through the mask is quantified using ultraviolet-visible (UV-vis) spectroscopy. Although performing the bacterial test would be required in order to certify the final mask, this aerosol test provides important information on the filter's performance. Microbes travel within exhaled breath, which contains aerosols; therefore, aerosol filtration is the focus of this work.

In the diagram shown in Figure 7 below, the general layout for the filtration test is shown. First, compressed air pressurized to 0.6 MPa is passed through a dehumidifier to dry the air at a rate of 24 L/min, which is in the range of average respiration [28]. The air then travels through the nebulizer which contains a concentrated methylene blue dye solution. Dyed aerosols are then pushed through the filter and collected in a beaker which is filled with a known quantity of water. The pressure difference is measured across the filter. After 5 minutes, the air flow is shut off. The same test is run again without the filter in order to obtain a reference dye sample from the top beaker.

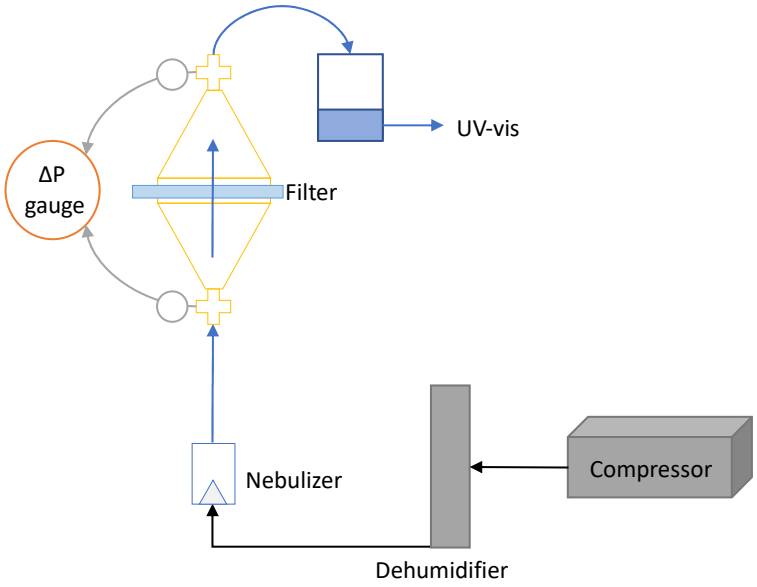

Figure 7. Test setup for filtration and breathability testing.

The liquid in the beaker is measured at the end of the test using a UV-vis spectrometer at a wavelength of 664 nm. The overall aerosol efficiency of the filter is determined from the difference in peak absorption between the liquid in the beaker with and without the filter in place using Equation 1 below:

$$\text{Efficiency} = 100\% * \left(1 - \frac{A_0 - A_1}{A_0}\right) \quad (1)$$

Where A_0 is the peak absorption of the reference liquid

A_1 is the peak absorption of the liquid tested with a filter

2.1.2 Breathability

The pressure difference across the mask is quantified in order to assess the breathability of the mask. With a lower the pressure difference across the filter, the user will have an easier time breathing while wearing the mask. In this work, the breathability of the mask is assessed via two tests: 1) breathability in the presence of aerosols generated during the filtration test, and 2) breathability with no aerosols present.

2.1.2.1 Breathability with aerosols challenge

During the filtration test mentioned previously, a pressure gauge measures the difference in pressure between the two sides of the filter as air containing dyed aerosols is passed through the filter. The maximum pressure difference across the filter is recorded, which typically occurred toward the end of the test as the aerosols accumulated on the surface of the filter, preventing air from passing through it. This test represents the worst-case use of the mask, wherein the user is expelling large quantities of aerosols, such as by coughing repeatedly.

2.1.2.2 Breathability without aerosols challenge

To mimic a more typical use case for such a filter, the breathability of the filter was assessed when only air passes across the filter. The test was set up in the same manner as the filtration test with aerosols, with the exception that the nebulizer was left empty. Air was once again passed through the sample at a rate of 24 L/min, and the pressure difference across the filter was recorded once the pressure value reached steady state, which typically occurred after 10 seconds.

2.1.3 Contact angle measurement

The hydrophobicity of a surface can be quantified by measuring the contact angle that it forms with water. A larger contact angle is associated with less wettability of the surface, and therefore a more hydrophobic surface. In this work, contact angle measurements are made to verify the hydrophobicity of the material, as well as to determine the effects of the chitosan coating on wettability. It is important that a surgical mask be hydrophobic; if water is able to wet the surface of the mask, it will permeate the fibers and reach to the other side. A hydrophobic surface prevents aerosol droplets from passing the filtration layer, thereby diminishing the risk of infection.

Contact angle measurements were made using the sessile drop method with 5 µL of distilled water. Five images were captured per surface using a Dino-Lite digital microscope. ImageJ was then used to measure the angle between the drop of water and the filter material. The filtration layer of a surgical mask was used as a reference material

as it is the standard this work is attempting to emulate. PLA-only and chitosan-coated PLA filters were characterized.

2.1.4 Scanning Electron Microscopy (SEM)

SEM is a spectroscopy technique that scans a surface using a focused beam of electrons to produce an image. The main components of SEM are the column, specimen chamber, and the display and operation section. First, the sample must be loaded into the chamber and vacuum must be pulled in order to minimize the scattering of the electrons on material other than the specimen. An electron gun then produces a beam of electrons which is then accelerated by a strong electric field. This electron beam is focused into a fine beam by an electromagnetic condenser lens. When the electron beam interacts with the surface of the specimen, different signals are generated, each giving useful information about the sample. One type of signal recorded is secondary electrons, which are low-energy electrons ejected from the k-shell of the specimen atoms through inelastic scattering interactions with the electron beam. The detection of secondary electrons provides information about the surface topology of the specimen [29].

In this work, SEM is used to visualize and characterize the morphology the prepared filters. Samples were sputter-coated with platinum in order render the surface of the insulating polymers conductive, allowing for a clear image to be obtained. The images were recorded using an accelerating voltage of 5.0 kV.

2.1.4.1 Fiber diameter calculations

MATLAB was used to analyze the SEM images and calculate fiber diameters for each filter type. First, the images were binarized to remove the background fibers, which appear lighter in color as compared to the foreground fibers. Then, a fiber diameter calculation was performed, adapted from a MATLAB script written by Rabbani et. al [30][31]. In this program, fibers are identified by the change in color from black (background) to white (fiber), and the average distance across the fibers are calculated. The 1% upper bound and lower bound outliers are removed from the calculation as they are assumed to result from image processing errors.

Fiber diameter calculations were performed on 5 images of each type of filter. The program was validated using the surgical filter. The surgical mask filter layer was calculated as having fiber diameters in the range of 1-2 μm, which falls in the expected range of 1-3 μm for meltblown surgical mask filters [32][33].

2.1.5 Brunauer-Emmett-Teller (BET) Method

Specific surface area and pore size were quantified using the BET method. For this analysis method, samples are placed in a vacuum chamber at an ambient temperature of 27 °C. Nitrogen gas is then pumped into the chamber and the quantity of gas molecules adsorbed onto the surface is quantified; this creates the adsorption isotherm. The pressure is then decreased, and the amount of gas desorbed is quantified. The specific surface area (S) is calculated per the Equation 2 below [34]:

$$S = \frac{W_m N A}{W_s M} \quad (2)$$

Where N is Avogadro's number (6.023 x 10^{23} atoms/mol)

M is the molecular weight of the adsorbate (g/mol)

A is the cross-sectional area of the adsorbate (16.2 Å for nitrogen)

W_s is the sample weight (g)

The pore volume can also be determined from the amount of gas adsorbed onto the surface of the material using the Barrett-Joyner-Halenda (BJH) method, which relies on the Kelvin model for pore filling, shown in Equation 3 below [35]. For this measurement, the quantity of nitrogen introduced to the chamber is increased past the point of a monolayer; as the pressure increases, the pores fill with nitrogen.

$$\ln \frac{P}{P_0} = \frac{2\gamma V}{r_k R T} \quad (3)$$

Where P/P_0 is the equilibrium pressure over the saturated vapor pressure

γ is the interfacial tension of liquid nitrogen

V is the molar volume of liquid nitrogen

r_k is the capillary radius

R is the gas constant

T is the ambient temperature

2.1.6 Differential Scanning Calorimetry (DSC)

Differential scanning calorimetry (DSC) can measure several quantities, including the specific heat capacity of a material, stability to oxidation, and temperature of chemical reaction. In this experiment, DSC is used to measure the change in heat flow in the polymer in response to change in temperature [36]. Heating and cooling cycles were performed on a polymer and reference sample separately in a nitrogen atmosphere. The change in heat flux was measured and the glass and melting onset temperatures were determined from the thermograms. Since the crystalline regions of polymers require more energy to melt, the transition temperatures are correlated to degree of crystallinity and therefore biodegradability.

Typically, the compostability of a material is determined by placing a sample in a composting medium and measuring the carbon dioxide produced over time as the microbes mineralize the degradation products. Because biodegradation testing requires up to 6 months of time, DSC was used to indirectly assess the biodegradability of the filter. DSC measurements were used to determine the crystallinity of the filter as compared to the raw PLA pellets, which are certified biodegradable. Since the sourced pellets are known to be compostable within a 3-month timeframe, the PLA filter would have to be equally or less crystalline than the raw pellets to ensure that they remain compostable.

Only the PLA filters with no chitosan coating were measured via DSC to simplify the measurement process. Chitosan has a faster degradation rate in composting conditions

than PLA, so PLA is the rate limiting factor of the material's degradation [37]. This assumption can be made because there is little interaction between the PLA and chitosan molecules [38]. We can therefore expect that the degradation of the material is dependent on cleavage of bonds in the individual polymers rather than bonds between polymers.

2.1.7 Electrostatic Voltmeter

An electrostatic voltmeter was used to detect static charge on the filters without physical contact. This meter can be used to measure voltage of a conductive surface, or charge density of an insulating surface. A sensor in the device uses a high voltage amplifier to increase the potential of the sensing probe until it matches the potential of the surface being measured. The output of the amplifier is then reported.

In order to assess the filters' ability to hold electrostatic charge over time, PLA and PLA/CS samples were fabricated using the spray pyrolysis method. These samples, along with a polypropylene surgical mask, were then charged in the electrospinning apparatus at 18 kV for 5 minutes. The electrostatic charge of the filters was measured over 4 hours using the AlphaLab surface voltmeter (Salt Lake City, UT, USA) at a distance of 2.54 cm from the samples. The room temperature was 20 °C and ambient relative humidity was at 36%.

2.1.8 Antiviral assessment using HCoV-OC43

This experiment was conducted in collaboration with the INRS – Institut Armand-Frappier Research Centre as they have the required biosafety certifications to work with live viruses. The antiviral activity of the filters was assessed via antiviral assay using HCoV-OC43, the virus responsible for the common cold. Like SARS-CoV-2, the virus used in this study is an enveloped coronavirus and part of the same genus. Thus, it is hypothesized that if the proposed antiviral mechanism can disrupt the envelope of HCoV-OC43, it can have the same effect on SARS-CoV-2. Further, it was desired to study HCoV-OC43 because although the common cold does not pose as much of a danger to society as COVID-19, it is endemic, and it could be desirable to minimize its transmission.

The experiment was designed such that it mimics real use of a mask as closely as possible. A droplet containing the virus comes into contact with the mask filter where it remains for several hours until the mask is handled by the user again, where the risk of transmission arises. First, filter samples were incubated with free reporter viruses of HCoV-OC43 for 2 hours at room temperature in a Dulbecco's Modified Eagle Medium (DMEM) culture medium. Samples were then used to infect HRT-18 cells. The degree of infection was measured 2 days later via luciferase assay. Several samples were compared: PLA/CS1 and PLA/CS2 were used to see if the antiviral effect becomes stronger with an increase in chitosan concentration in the coating. A PLA sample without the chitosan coating was used as a control. Finally, an empty cell was incubated with the virus to ensure the PLA filters were not responsible for any antiviral effect.

3 EXPERIMENTAL RESULTS

This section contains the results of the experiments previously described, and discusses the significance of these results.

3.1 Filtration and Breathability

The aerosol filtration of the surgical, PLA, PLA/CS1 and PLA/CS 2 filters are shown in Table 2 below. All filters demonstrate similar filtration values as the benchmark surgical mask filter of approximately 98%. The pressure difference across the filter corresponds to the breathability of the filter; a lower pressure differential is desired in order to achieve a filter which is more comfortable to the user. The PLA, PLA/CS 1 and PLA/CS2 do not have a statistically significant difference in breathability as compared to the surgical mask.

Table 2. Average filtration and pressure differential with and without aerosol challenge showing the 95% confidence interval for the tested filters.

Material	Average Filtration (%)	Pressure Differential with aerosols (Pa)	Pressure Differential without aerosols (Pa)
Surgical	97.7 ± 1.1	126 ± 23	15 ± 1
PLA	97.9 ± 1.6	164 ± 38	12 ± 2
PLA/CS1	97.9 ± 1.8	196 ± 53	11 ± 5
PLA/CS2	97.6 ± 2.0	250 ± 75	14 ± 4

There is larger confidence interval for the PLA, PLA/CS 1, and PLA/CS2 samples due to variability induced during filter production. The surgical filter, on the other hand, is produced commercially and has a uniform filter distribution, and therefore has a more uniform pressure differential from one filter to another. Further, the spray pyrolysis method used to prepare the PLA samples can result in the formation of voids in the filter. When the filter is coated in chitosan, these voids may be covered by the chitosan film, thereby increasing the resistance to air flow. Since this coating is not present in the PLA filter, these samples may demonstrate a lower pressure differential. Despite the addition

of the chitosan coating, PLA/CS 1 and PLA/CS2 remain in the comfortable range for breathability. The coating, therefore, does not fill all the voids in the filter.

3.1 **Contact Angle**

The hydrophobicity of the filter samples was quantified using contact angle measurements and compared to the benchmark surgical PP filter. Such contact angle images are shown in Figure 8 below.

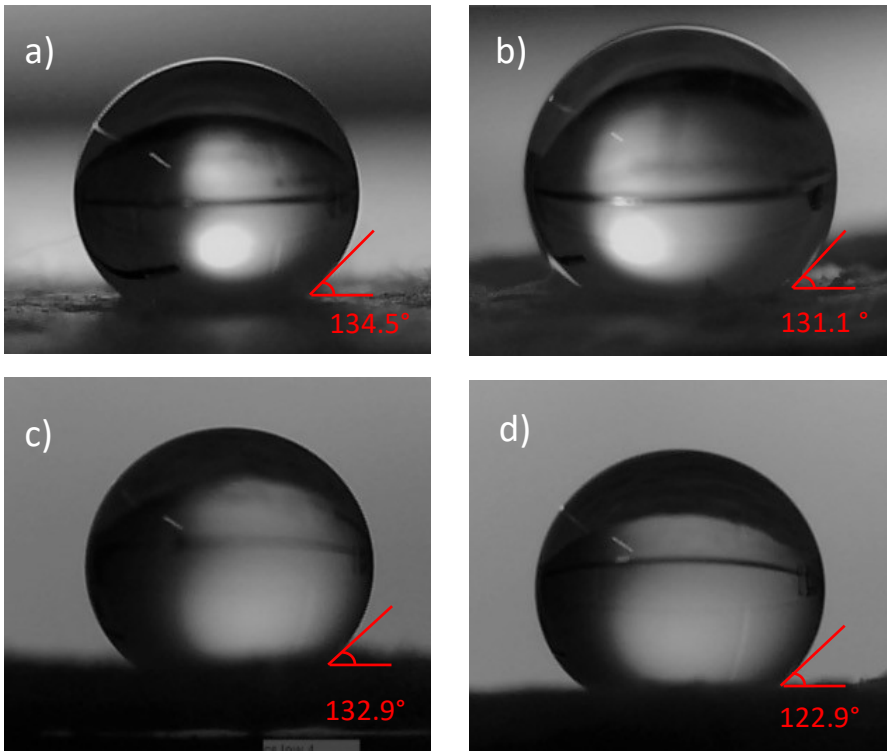

Figure 8. **Sample contact angle images for the surgical PP (a), PLA (b), PLA/CS1 (c), and PLA/CS 2 (d) filters.**

Figure 9 below summarizes the contact angle measurements made for the PLA, PLA/CS1, and PLA/CS2 filters as compared to the commercially produced surgical mask filtration layer. Five samples were taken for each filter type. All filters demonstrate hydrophobic behavior, which is important in minimizing the permeation of aerosols through the mask. The filtration layer of the surgical filter, the PLA filter, and the PLA/CS1 filter do not have statistically significant contact angles at the p=0.05 level. However,

PLA/CS2 demonstrates a statistically significant decrease in contact angle as compared to the filters with less or no chitosan, indicating that the surface has a slightly higher wettability. This increase in wettability is likely due to the chitosan's hydrophilic property, as well as it forming films between the PLA fibers. These films diminish the effect of the fibers' microstructure on the surface energy of the surface. Thus, aerosols deposited on the surface of the filter will permeate the PLA/CS2 filter more rapidly than the filters with less chitosan. Despite this, however, the PLA/CS2 samples demonstrate relatively hydrophobic surface properties.

The increase in wettability does, however, present an advantage in the compostability of the mask. Because the first mechanism of PLA decomposition is hydrolysis of the O-H bonds in the polymer, the increase in water permeation of the mask will accelerate decomposition of the mask. The PLA/CS2 filter, therefore, would be expected to decompose more rapidly than the PLA/CS1 and PLA filters while remaining hydrophobic.

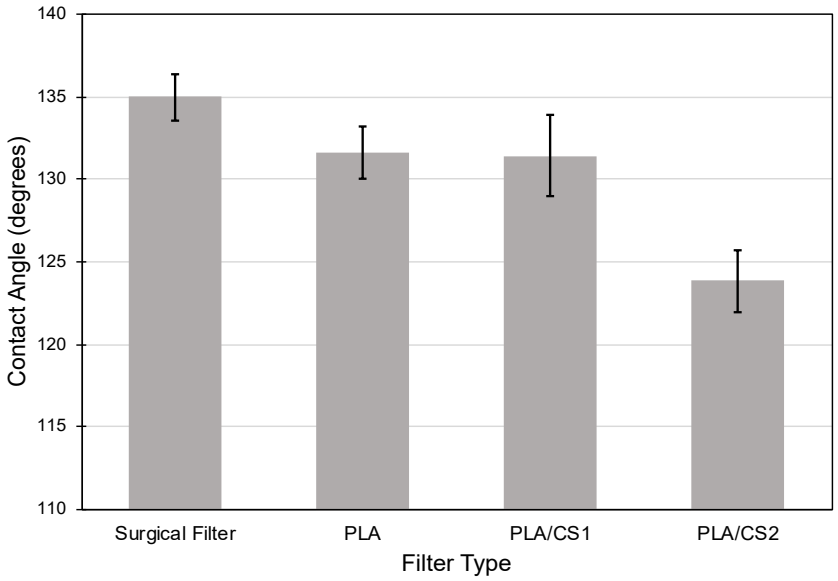

Figure 9. **Contact angle measurements for the tested filters. The error bars designate the 95% confidence interval. Note: the y-axis begins at 110° to better demonstrate differences between samples.**

3.2 **Fiber Morphology**

In order to produce fibers in a rapid and facile manner, spray pyrolysis of the polymer solution was used as opposed to the typical method of melt-blowing, which requires expensive equipment. Figure 10 below demonstrates the differences in the morphology of the resulting solvent-cast PLA fibers as compared to meltblown PP fibers from a standard surgical mask. Notably, the meltblown fibers are more regular and linear as compared to the solvent-cast fibers. Further, the meltblown fibers are evenly distributed, whereas the solvent-cast fibers tend to agglomerate into bundles. Thus, in the solvent-cast method of producing polymer fibers, two fiber diameters can be characterized: the diameters of the individual fibers, as well as the diameters of the fiber bundles.

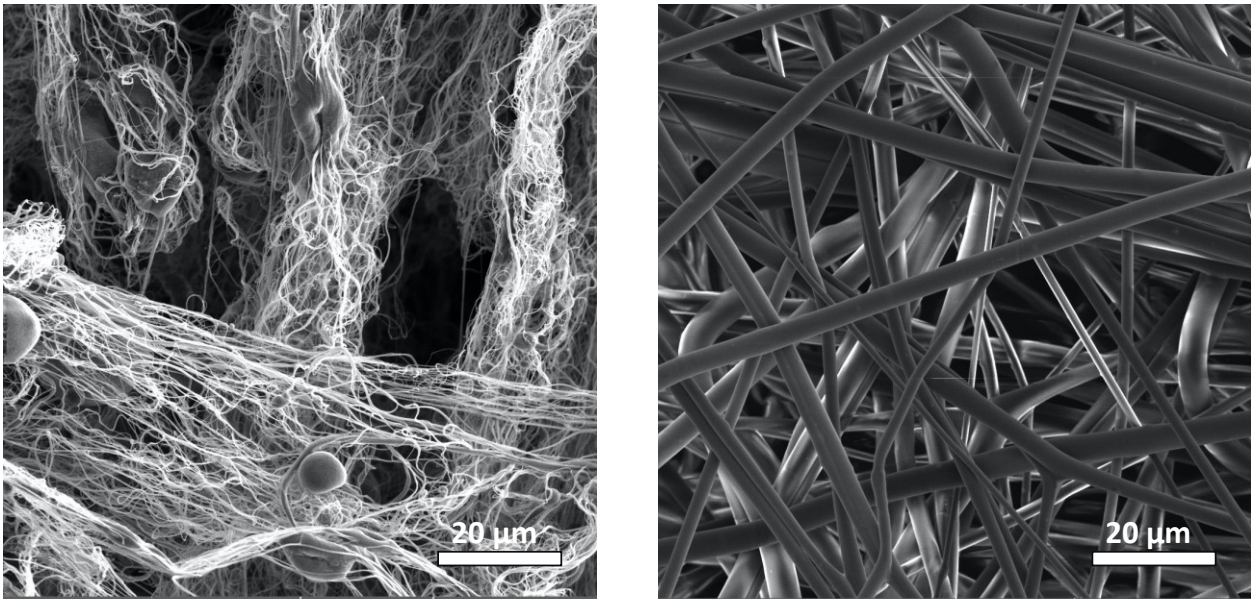

Figure 10. SEM images of solvent-cast PLA fibers (left) and meltblown PP (right).

The bundles were measured using ImageJ and found to have an average bundle diameter of 39 ± 11 µm, calculated from five samples. These bundles present a disadvantage in the filtration performance of the mask; since the subsequent layers of fibers tend to adhere preferentially to each other, voids are left behind through which aerosols or particles could pass.

Figure 11 below reveals the morphology of the PLA fibers after the application of chitosan. Rather than coat each PLA fiber individually, the chitosan forms a film between some of the fibers. The concentration of the chitosan solution used is sufficiently low such that it does not completely block all voids between fibers, thereby allowing air to pass. Small islands are present in this chitosan film, which is likely due to the film shrinking upon drying as the water from the chitosan solution evaporates.

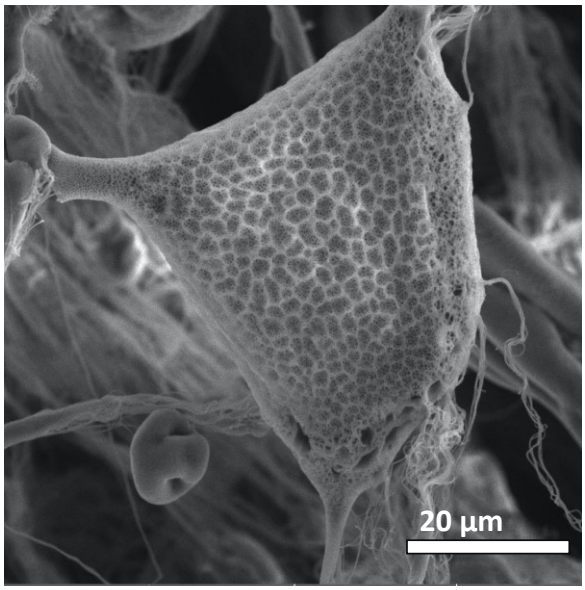

Figure 11. Solvent-cast PLA fibers coated in the chitosan solution.

The diameters of the individual fibers were then calculated using MATLAB. As shown in Figure 12 below, the fibers of the surgical mask have a larger diameter than those of the three filters prepared in this work. This is likely due to the difference in production methods; the surgical filter is prepared via industrial meltblowing, while the other three are prepared via lab-scale solvent spray pyrolysis. There is no statistically significant difference between the diameters of the three PLA-based filters. This further suggests that the chitosan does not coat individual PLA fibers, but rather forms intermittent films between certain fibers in the filter.

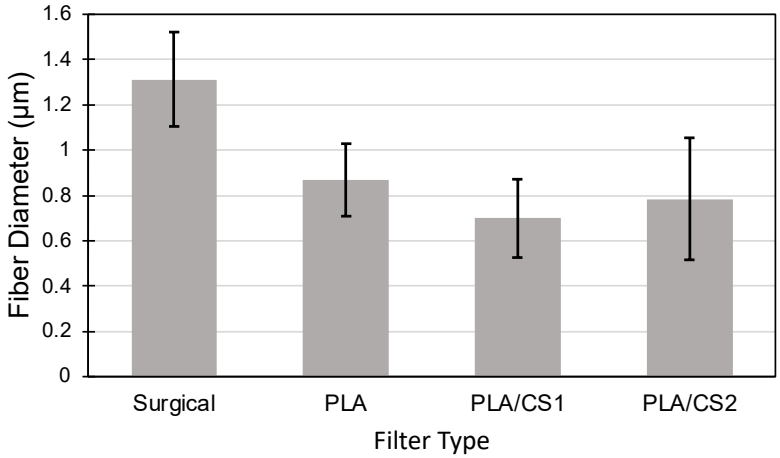

Figure 12. **Fiber diameters for various filter types measured from SEM images using MATLAB. Error bars show the standard deviation.**

Figure 13 below shows fiber diameter distributions for the filters produced as compared to a surgical mask. All samples reveal a left-skewed unimodal distribution. The surgical mask filter layer was calculated as having fiber diameters in the range of 1-2 µm, which falls in the expected range of 1-3 µm for meltblown surgical mask filters [32][33]. One can conclude that the fiber diameters calculated by this MATLAB script are accurate.

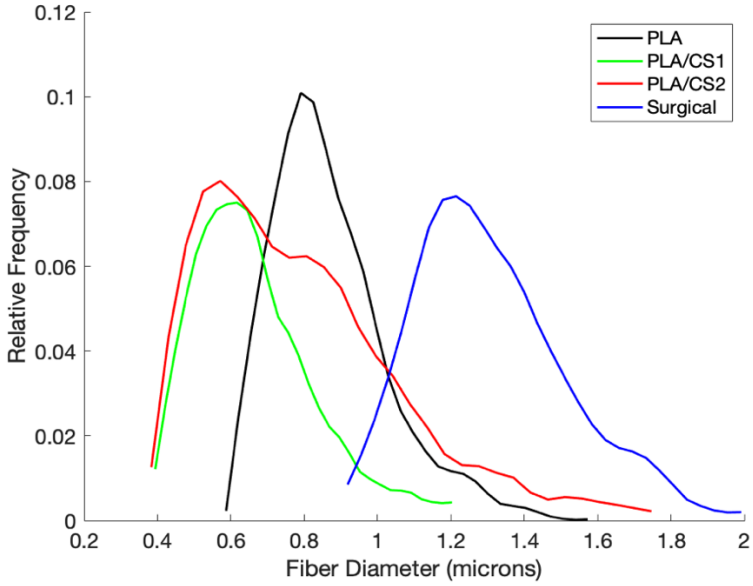

Figure 13. **Histogram showing fiber diameter distributions for the various types of filters created, as compared to surgical mask fibers.**

3.3 **Specific Surface Area and Pore Volume**

BET was used to quantify the specific surface area and pore volume of the filters. Figure 14 below shows the resulting specific surface areas for the various filters, using the multipoint BET method to calculate the values, in addition to the pore volume calculated from the BJH cumulative adsorption curves. Despite the creation of smaller fibers in the sprayed samples, the PLA was found to have a lower surface area than the surgical mask. The two chitosan samples demonstrate similar surface areas. The pore volume data coincide with the surface area calculations for specific surface area; the PLA sample demonstrates the lowest pore volume, while the PLA/CS1 and PLA/CS2 have more than double the pore volume.

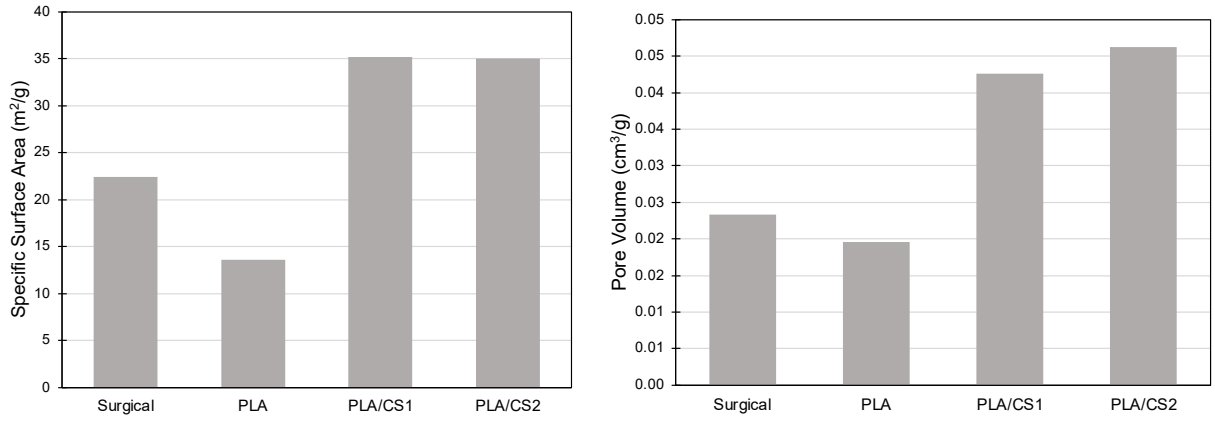

Figure 14. **Specific surface area of the different filter types calculated using multipoint BET method (left), pore volume calculated from BJH cumulative adsorption (right).**

These data do not align with the fiber diameter measurements and morphology observed via SEM. Samples with smaller fibers, like the PLA sample, were expected to have a greater specific surface area and pore volume. A likely reason for this discrepancy could arise from issues with the BET test. As shown in Figure 15 below, the desorption curves are negative. Typically, a positive hysteresis is expected for the adsorption/desorption curves in a BET experiment since some nitrogen gas molecules remain entrapped in the pores of the material during desorption. Although the adsorption isotherm, which was used to calculate the specific surface area and pore volume, demonstrates the expected

behavior, the negative hysteresis indicates that there may have been an issue in the experiment, making the results unreliable.

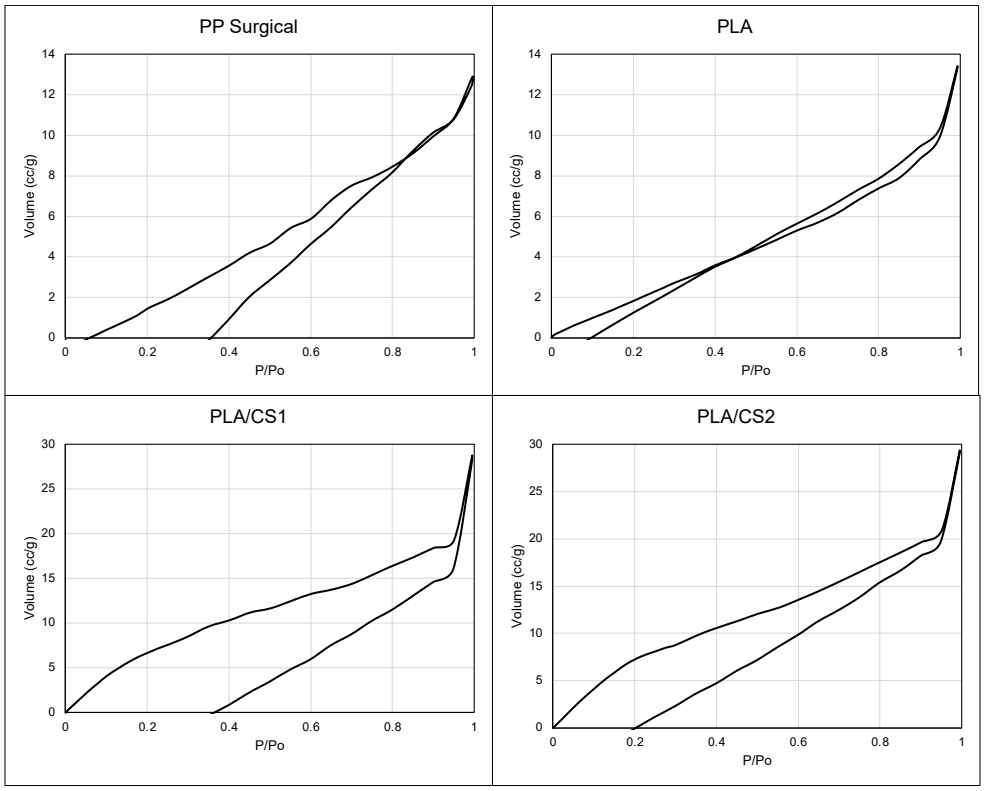

Figure 15. Absorption and desorption curves for PP, PLA, PLA/CS1, and PLA/CS2 filters as measured via BET method.

3.4 **Crystallinity**

EN-13432 is the governing standard in Europe for compostable bioplastics and is recognized globally. Per this standard, a plastic is considered compostable if it reaches a decrease in mass of 90% after 3 months [39]. The PLA used in this work, Total Corbion's L105 grade of PLA, is certified compostable per EN-13432 up to a thickness of 2.3 mm [40]. As a preliminary verification of the filters' compostability, the crystallinity of the sprayed fibers is assessed via DSC. The goal of this study is to verify that the processing of our fibers does not increase the crystallinity of the material compared to the as-received PLA pellets, as this would likely decrease the degradation rate. Thus, if the degradation

rate decreases, it is possible that the final product will not meet the requirements for compostability per EN-13432.

This report only assesses the crystallinity and degradation of the PLA component of the filter since chitosan has a faster degradation rate than PLA, degrading in a matter of days [37][41]. Furthermore, because chitosan is a hydrophilic polymer, its incorporation into the filter helps draw water thereby accelerating hydrolysis of the PLA [42]. Thus, the degradation of PLA is the rate-limiting factor. The first scan thermograms obtained for the as-received pellets and the sprayed fibers are shown in Figure 16 below.

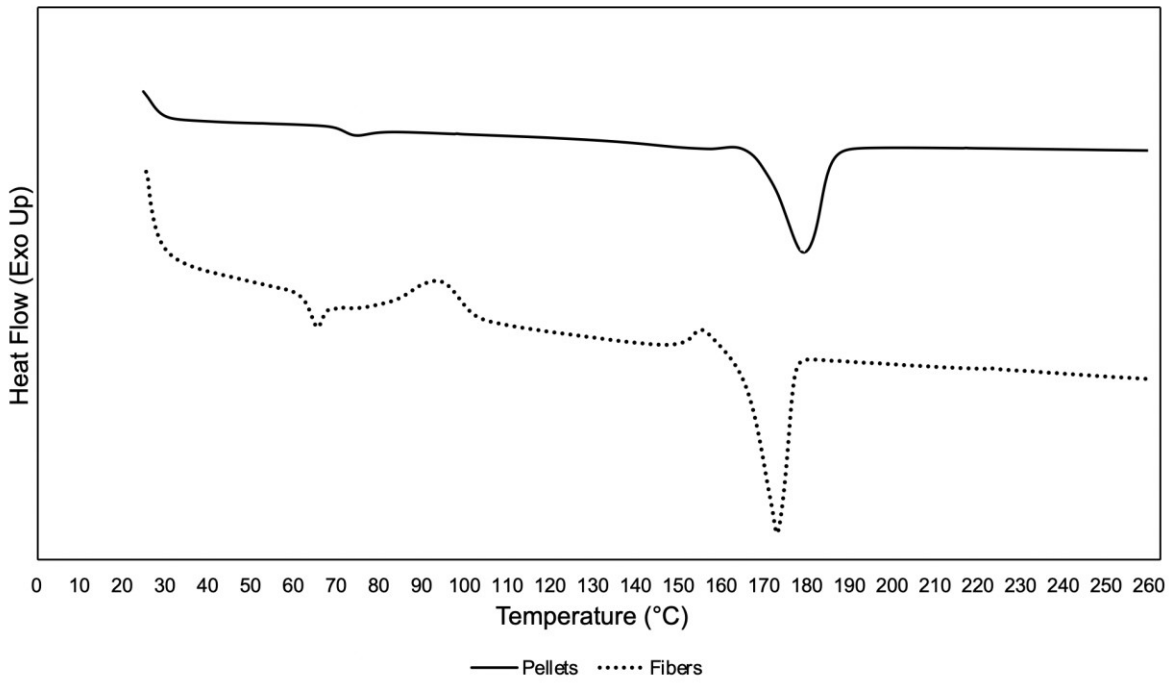

Figure 16. **Thermograms for Total Corbion Luminy105 PLA as-received in pellet form (solid line) and transformed into fibers via solvent-casting (dotted line). Heating rate was set to 10.00 °C/min and measurements were made under nitrogen atmosphere.**

The crystallinity, X_c, of each sample was calculated from the heat of enthalpy measured during melting, shown in Equation 4 below [43]:

$$X_c = \frac{H_s}{H_o} \tag{4}$$

Where H_s is the enthalpy of melting of the sample

H_o is the standard enthalpy of melting for 100% crystalline material

Using the heat of enthalpy for 100% crystalline PLA as 93.7 J/g [18] and Equation 4, the crystallinity of the PLA pellets is determined to be 53.3% while that of the fibers is 59.5%. It should be noted, however, that this crystallinity is calculated during the melting of crystallites. As shown in the thermograms, the fibers undergo two small crystallization peaks at 95 °C and 155 °C as the fibers rearrange themselves into a more stable configuration. Thus, this crystallinity value does not necessarily reflect the crystallinity at lower temperatures.

Transition temperatures of the polymer can give insight into the room temperature crystallinity of the fibers and pellets. Table 3 below summarizes the transition onset temperatures for each sample. The sprayed fibers demonstrate lower glass transition and melting temperatures than the pellet form, suggesting a more amorphous structure. This is likely due to the rapid precipitation of the polymer due to solvent evaporation, which yields a more amorphous structure than the as-received polymer. Fast precipitation results in a greater free volume in the material, which explains the presence of a crystallization peak immediately after the glass transition of the fiber sample; this crystallization peak did not occur in the pellet sample since the polymer chains were already in an organized and stable structure.

Table 3. Transition temperatures for pellets and fibers.

	T_g (°C)	T_m (°C)
PLA Pellets	69.62	169.32
PLA Fibers	62.61	165.84

The thermograms suggest that the fibers are more amorphous at temperatures below the glass transition as compared to the as-received pellets. This is favourable for degradation in compost conditions because the higher free volume content allows for greater moisture ingress, which results in higher hydrolysis rates. One can therefore assume that the fibers will not take longer to degrade as compared to the original polymer certified by EN-13432. To further confirm this, XRD can be used to directly measure the crystallinity of the

samples. It should be noted that in order to assume that the PLA/CS filters will be compostable, the following assumptions are made:

1. The chitosan in this filter will not decrease the degradation rate
2. The solvent is completely evaporated in the final product

Should the PLA filter be made via meltblowing rather than solvent pyrolysis, it is expected that the meltblowing process would induce similar stresses on the PLA which would render it more amorphous than the as-received pellets. Previous works show that a similar decrease in T_g and T_m will be present in meltblown PLA due to the rapid cooling of the melted polymer [44]. A degradation study would have to be performed when the processing parameters of the filter are determined in order to certify the compostability of the filter.

3.5 Electrostatic Charge Retention

The ability of a polymer to become charged and retain this charge is related to its dielectric constant, ε_r. With a high ε_r, a polymer will charge rapidly but is susceptible to losing this charge quickly. Table 4 below shows the dielectric constants of the polymers assessed in this experiment.

Table 4. Dielectric Constants of PP and PLA.

Polymer	Dielectric Constant (1 kHz)
Polypropylene	2.2 [45]
Poly(lactic acid)	3.2 [4]

As shown in Table 5 below, the PLA and PLA/CS samples were charged to a similar degree after being exposed to the same electric field, while the PP surgical filter did not exhibit as high of a charge density. This is because the PLA has a greater capacity to become charged due to its polar groups. The structure of polypropylene consists of repeating units of -CH2; PLA, on the other hand, has a double bonded oxygen, which

creates a dipole in the polymer chain. This dipole can therefore bind more strongly to the applied charges as compared to the polypropylene.

Table 5. Initial charge density of filters immediately after charging.

Filter Type	Initial Charge Density (nC/cm^2)
PP	0.066
PLA	0.145
PLA/CS1	0.151

Figure 17 below demonstrates that the PLA and PLA/CS masks had better charge retention than the surgical PP mask over a 4-hour period; the PLA and PLA/CS1 mask demonstrated a 22% and 32% decrease in charge, respectively, while the PP surgical filter demonstrated a decrease of 38%.

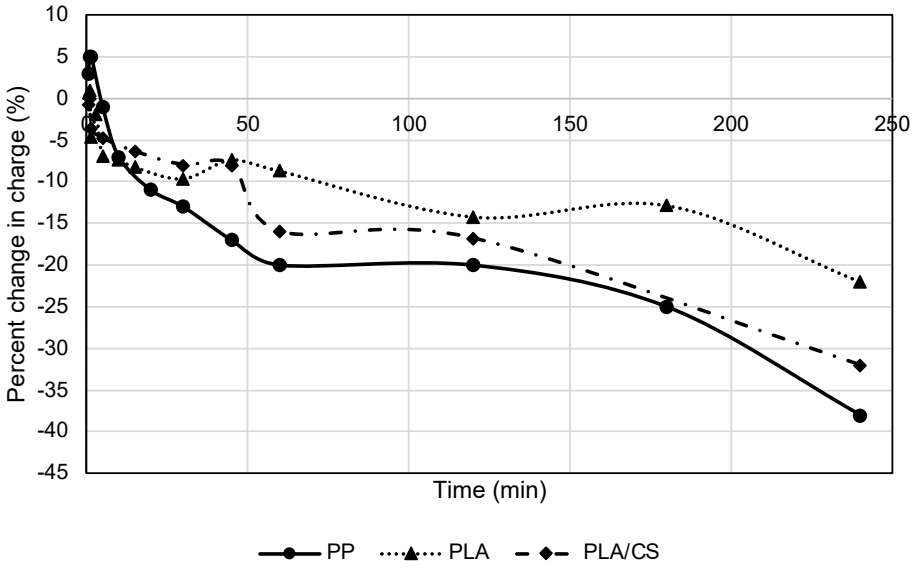

Figure 17. Change in electrostatic charge of the PP, PLA, and PLA/CS1 samples over a four-hour isothermal period.

Differences in charge retention between the PLA and PP masks could be attributed to differences in crystallinity of the polymers. Because charges are trapped by crystallites in

the polymer, a more crystalline polymer will have a greater charge retention than a more amorphous one. Although the crystallinity of this specific PP mask was not quantified in this work, other research has demonstrated that the crystallinity of PP surgical masks is relatively low, at approximately 21% at 20 °C [32]. The PLA fibers prepared in this work, however, have a degree of crystallinity of 59.5%, as was calculated from the DSC data. It is possible, therefore, that the PLA filters' greater charge concentration and retention are attributed to a higher crystallinity.

The measurements above reflect a single experiment conducted at 20 °C and relative humidity of 36%. Because the humidity could not be controlled, the experiment could not be easily repeated on various days to verify the results. For a better experiment and more reliable results, a humidity-controlled chamber in which measurements can be made would have to be used, or all samples would have to be tested at once.

3.6 **Antiviral assessment**

The results from the first trial of the antiviral testing are shown in Figure 18 below. There is no statistically significant difference between the reference, control (PLA) and PLA/CS1 samples. However, the PLA/CS2 sample, with a high chitosan concentration, demonstrates a 0.83-fold reduction in infectivity compared to the reference sample with no textile. This represents a 0.61-fold reduction compared to the PLA control sample. These results do not correspond to significant antiviral properties; typically, a decrease in infectivity of at least 10-fold is expected for a material to be considered antiviral. Thus, the results of this experiment do not demonstrate antiviral behaviour.

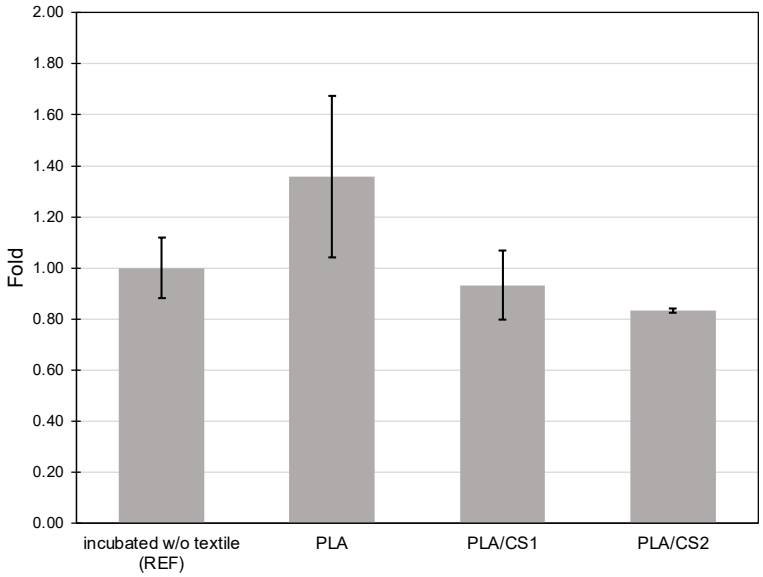

Figure 18. First trial of antiviral assay with HCoV-OC43.

The experiment was repeated with a more dilute virus concentration. The reasoning behind this change is that there may have been too high of a number of viruses in contact with the sample in comparison to the number of charged sites on the chitosan. The results for this trial are shown in Figure 19 below. These data are inconclusive since the samples containing chitosan had a higher number of active viruses as compared to the PLA sample. As previously mentioned, the values recorded are relatively similar for all samples; not enough of a viral infectivity reduction was recorded to draw any conclusions from this test.

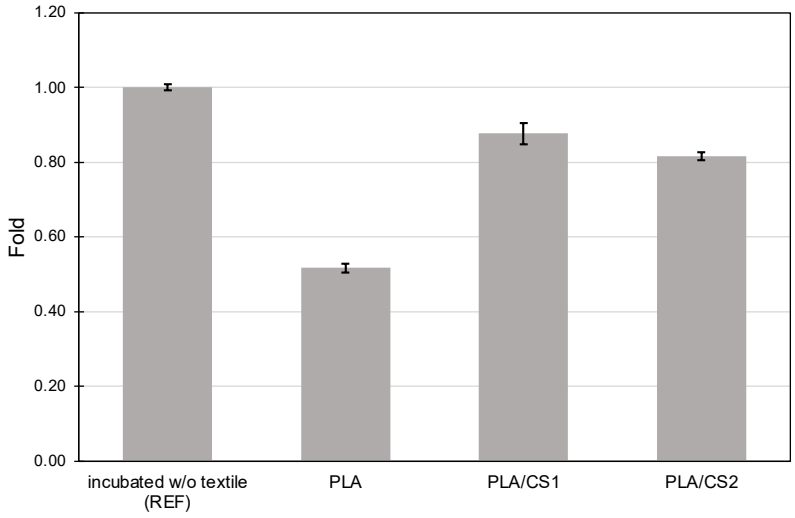

Figure 19. Second trial of antiviral assay with HCoV-OC43 using a more dilute virus solution.

Further studies could be conducted using a lower concentration of the virus. Additionally, chitosan could be tested alone in order to maximize its concentration, thus elucidating whether the biopolymer as any antiviral effect on HCoV-OC43. Furthermore, it is possible that the solution used to suspend the viruses could inhibit the antiviral activity of the chitosan. Chitosan's antiviral activity is not the same across all culture mediums; M9 has been shown to work well with chitosan, whereas when Luria Broth (LB) medium is used, chitosan's antiviral effect is diminished [46]. The culture medium used in this work is DMEM, which has not been readily studied in its effect on the antiviral activity of chitosan.

4 APPLICATIONS

4.1 Integration into existing mask assembly lines

This work has demonstrated the potential of biopolymers for use in advanced technologies. Although only the filtration layer is discussed herein, the two exterior layers could also be made with PLA using the same spunbond process currently used in surgical masks. To make a complete mask, a biodegradable nose bridge and ear loop material would be necessary. For added protection, the PLA fibers could be made via electrospinning, wherein the polymer solution is drawn from a syringe using a strong

electric field rather than air pressure used in this work. With electrospinning, nanofibers can be formed, thereby improving the filtration performance of the overall mask [47] [48].

4.1 Air filtration

The same principles that would make this filter applicable for surgical masks would make it suitable for air filtration. As industrialization increases the concentration of particulate matter in the air, it is becoming more important than ever to filter the air coming into buildings and home in order to prevent these particles from entering people's airways. These particles, which vary in size, can be filtered mechanically and electrostatically. Furthermore, it could be beneficial to inactivate microbes such as viruses and bacteria using these filters in high-traffic areas, such as offices and shopping centers, in order to further minimize the transmission of diseases. Although these filters are not replaced as often as surgical masks, there is still great benefit in making these compostable in order to minimize the waste they produce [47].

4.2 Biomedical applications

The facile method for fiber production described in this work could be well-suited for the biomedical industry as well. Fibrous, biodegradable scaffolds are often used for tissue regeneration as they provide sufficient surface area upon which cells can adhere [48]. Furthermore, PLA's biodegradability and low toxicity makes it an good candidate for minimizing immune response and increasing cell viability [49]. The use of spray pyrolysis as a method of fabrication could be used for accessible, lab-scale production of such scaffolds as opposed to the use of the more expensive electrospinning, which is currently used. In the case of skin tissue regeneration, where the risk of infection is high, the incorporation of chitosan as an antimicrobial agent could minimize this risk. Work by Gomaa et al. has demonstrated the successful growth of mouse cells on such a nanofiber mat, using a different antimicrobial agent, thymoquinone [50].

5 CONCLUSIONS AND PERSPECTIVES

5.1 Conclusions

In this work, a compostable filtration material is produced via an inexpensive and accessible process. Preliminary tests reveal that this nonwoven fiber material performs similarly to the typical polypropylene surgical mask filtration layer with respect to filtration and breathability. Additionally, this spray pyrolysis process was shown to produce smaller fibers than the meltblown fibers of the surgical mask. This process resulted in a slight decrease in crystallinity as compared to the raw PLA, potentially resulting in a faster degradation time. Sufficient crystalline regions remain in the fibers such that they can retain charge; this, combined with the electret properties of PLA, result in a mask which can retain charge better than the existing polypropylene surgical mask. A chitosan coating was added which did not have a significant impact on hydrophobicity of the overall surface. The antiviral activity of this chitosan coating was tested against HCoV-OC43, however the experiment was inconclusive.

5.2 Perspectives

Although this work has demonstrated the feasibility of a compostable and antimicrobial surgical mask filter, some further work would be necessary prior to the commercialization of this product. Notably, a biodegradation test in composting conditions would be necessary to verify the compostability of the filter. Furthermore, filtration testing using bacteria and particles of known diameters would be important in order to understand how the material's filtration performance is affected by particle size. Lastly, to verify the antiviral behavior of chitosan, more testing would be necessary using the live virus, employing different inoculation mediums or methods.

While some grades of PLA can be composted industrially, not all industrial composting facilities accept compostable plastics because they are difficult to degrade in an efficient timeframe. Future works should study methods or additives to further enhance the rate of degradation of the PLA, whether through treatment or the use of additives. Furthermore,

for rapid integration into existing supply chains and manufacturing streams, it would be beneficial to reproduce this work using the typical method for nonwoven filter preparation – meltblowing. Not only would this reduce the obstacles for integration of this new product, but it would also eliminate the need for use of a solvent, thereby further reducing the environmental impact of this product.

Additionally, different methods for achieving antiviral activity of this mask could be assessed. For example, the use of nanoparticles as opposed to a coating could limit the increase in wettability caused by the chitosan coating, while benefiting from the high surface area imparted by nanoparticles. The use of nanoparticles would have to be assessed from a safety perspective if used in a mask due to potential inhalation of the particles, although this method would remain well suited for other types of surfaces where inhalation does not pose an issue, such as coatings for frequently touched surfaces.

6 REFERENCES

[1] H. F. Lorentzen, T. Benfield, S. Stisen, and C. Rahbek, “COVID-19 is possibly a consequence of the anthropogenic biodiversity crisis and climate changes,” p. 6.

[2] “Medical Face Mask Market - Global Outlook and Forecast 2020-2025,” Arizton Advisory and Intelligence, Jun. 2020. Accessed: Apr. 10, 2021. [Online]. Available: https://www.marketresearch.com/Arizton-v4150/Medical-Face-Mask-Global-Outlook-13345767/

[3] N. B. Rodríguez, G. Formentini, C. Favi, and M. Marconi, “Environmental implication of personal protection equipment in the pandemic era: LCA comparison of face masks typologies,” *Procedia CIRP*, vol. 98, pp. 306–311, Jan. 2021, doi: 10.1016/j.procir.2021.01.108.

[4] “Effectiveness of Masks: Fast Answers with Automated SEM Analysis,” *Nanoscience Instruments*. https://www.nanoscience.com/applications/materials-science/effectiveness-of-masks-fast-answers-with-automated-sem-analysis/ (accessed Oct. 11, 2021).

[5] E. Hossain *et al.*, “Recharging and rejuvenation of decontaminated N95 masks,” *Physics of Fluids*, vol. 32, no. 9, p. 093304, Sep. 2020, doi: 10.1063/5.0023940.

[6] F23 Committee, “Specification for Performance of Materials Used in Medical Face Masks,” ASTM International. doi: 10.1520/F2100-19.

[7] R. Y. Siddiquie, A. Gaddam, A. Agrawal, S. S. Dimov, and S. S. Joshi, “Anti-Biofouling Properties of Femtosecond Laser-Induced Submicron Topographies on Elastomeric Surfaces,” *Langmuir*, vol. 36, no. 19, pp. 5349–5358, May 2020, doi: 10.1021/acs.langmuir.0c00753.

[8] 2003 Jun 01, “Principles of Physiology and Respirator Performance -,” *Occupational Health & Safety*. https://ohsonline.com/articles/2003/06/principles-of-physiology-and-respirator-performance.aspx (accessed Sep. 13, 2021).

[9] J. Zhang, G. Chen, G. S. Bhat, H. Azari, and H. Pen, “Electret characteristics of melt-blown polylactic acid fabrics for air filtration application,” *Journal of Applied Polymer Science*, vol. 137, no. 4, p. 48309, Jan. 2020, doi: 10.1002/app.48309.

[10] “Electrocharging Face Masks with Corona Discharge Treatment,” *OIST Groups*, Dec. 22, 2020. https://groups.oist.jp/nnp/electrocharge-mask (accessed Oct. 11, 2021).

[11] E. Motyl, “Effect of Air Humidity on Charge Decay and Lifetime of PP Electret Nonwovens,” *Fibres & Textiles in Eastern Europe*, 2006.

[12] Z. Adamczyk, P. Batys, and J. Barbasz, “SARS-CoV-2 virion physicochemical characteristics pertinent to abiotic substrate attachment,” *Current Opinion in Colloid & Interface Science*, vol. 55, p. 101466, Oct. 2021, doi: 10.1016/j.cocis.2021.101466.

[13] X. Ou *et al.*, “Characterization of spike glycoprotein of SARS-CoV-2 on virus entry and its immune cross-reactivity with SARS-CoV,” *Nature Communications*, vol. 11, no. 1, p. 1620, Mar. 2020, doi: 10.1038/s41467-020-15562-9.

[14] Turoňová Beata *et al.*, “In situ structural analysis of SARS-CoV-2 spike reveals flexibility mediated by three hinges,” *Science*, vol. 370, no. 6513, pp. 203–208, Oct. 2020, doi: 10.1126/science.abd5223.

[15] P. H. Pawłowski, “Charged amino acids may promote coronavirus SARS-CoV-2 fusion with the host cell,” *AIMSBPOA*, vol. 8, no. 1, Art. no. biophy-08-01-008, 2021, doi: 10.3934/biophy.2021008.

[16] J. Haldar, D. An, L. Álvarez de Cienfuegos, J. Chen, and A. M. Klibanov, “Polymeric coatings that inactivate both influenza virus and pathogenic bacteria,” *Proc Natl Acad Sci USA*, vol. 103, no. 47, p. 17667, Nov. 2006, doi: 10.1073/pnas.0608803103.

[17] V. A. Kabanov and A. A. Yaroslavov, “What happens to negatively charged lipid vesicles upon interacting with polycation species?,” *Journal of Controlled Release*, vol. 78, no. 1, pp. 267–271, Jan. 2002, doi: 10.1016/S0168-3659(01)00496-5.

[18] B. B. Hsu, S. Y. Wong, P. T. Hammond, J. Chen, and A. M. Klibanov, “Mechanism of inactivation of influenza viruses by immobilized hydrophobic polycations,” *Proceedings of the National Academy of Sciences*, vol. 108, pp. 61–66, 2010.

[19] V. S. Mandala, M. J. McKay, A. A. Shcherbakov, A. J. Dregni, A. Kolocouris, and M. Hong, “Structure and drug binding of the SARS-CoV-2 envelope protein transmembrane domain in lipid bilayers,” *Nature Structural & Molecular Biology*, vol. 27, no. 12, pp. 1202–1208, Dec. 2020, doi: 10.1038/s41594-020-00536-8.

[20] M. Safarzadeh, S. Sadeghi, M. Azizi, M. Rastegari-Pouyani, R. Pouriran, and M. Haji Molla Hoseini, “Chitin and chitosan as tools to combat COVID-19: A triple approach,” *International Journal of Biological Macromolecules*, vol. 183, pp. 235–244, Jul. 2021, doi: 10.1016/j.ijbiomac.2021.04.157.

[21] A. Milewska *et al.*, “HTCC: Broad Range Inhibitor of Coronavirus Entry,” *PLOS ONE*, vol. 11, no. 6, p. e0156552, Jun. 2016, doi: 10.1371/journal.pone.0156552.

[22] F. Sami El-banna, M. E. Mahfouz, S. Leporatti, M. El-Kemary, and N. A. N. Hanafy, “Chitosan as a Natural Copolymer with Unique Properties for the Development of Hydrogels,” *Applied Sciences*, vol. 9, no. 11, 2019, doi: 10.3390/app9112193.

[23] T. Kullmann, I. Barta, B. Antus, M. Valyon, and I. Horváth, “Environmental temperature and relative humidity influence exhaled breath condensate pH,” *Eur Respir J*, vol. 31, no. 2, p. 474, Feb. 2008, doi: 10.1183/09031936.00128007.

[24] S. N. Kulikov, S. N. Chirkov, A. V. Il'ina, S. A. Lopatin, and V. P. Varlamov, "Effect of the molecular weight of chitosan on its antiviral activity in plants," *Applied Biochemistry and Microbiology*, vol. 42, no. 2, pp. 200–203, Mar. 2006, doi: 10.1134/S0003683806020165.

[25] V. N. Davydova *et al.*, "Chitosan antiviral activity: Dependence on structure and depolymerization method," *Applied Biochemistry and Microbiology*, vol. 47, no. 1, pp. 103–108, Jan. 2011, doi: 10.1134/S0003683811010042.

[26] L. W. McKeen, "13 - Environmentally Friendly Polymers," in *Permeability Properties of Plastics and Elastomers (Third Edition)*, L. W. McKeen, Ed. Oxford: William Andrew Publishing, 2012, pp. 287–304. doi: 10.1016/B978-1-4377-3469-0.10013-X.

[27] N. F. Zaaba and M. Jaafar, "A review on degradation mechanisms of polylactic acid: Hydrolytic, photodegradative, microbial, and enzymatic degradation," *Polymer Engineering & Science*, vol. 60, no. 9, pp. 2061–2075, Sep. 2020, doi: 10.1002/pen.25511.

[28] F23 Committee, "Test Method for Evaluating the Bacterial Filtration Efficiency (BFE) of Medical Face Mask Materials, Using a Biological Aerosol of Staphylococcus aureus," ASTM International, ASTM F2101-19. doi: 10.1520/F2101-19.

[29] "What is SEM? Scanning Electron Microscopy Explained," *Accelerating Microscopy*, Nov. 14, 2019. https://www.thermofisher.com/blog/microscopy/what-is-sem-scanning-electron-microscopy-explained/ (accessed Nov. 02, 2021).

[30] A. Rabbani and S. Salehi, "Dynamic modeling of the formation damage and mud cake deposition using filtration theories coupled with SEM image processing," *Journal of Natural Gas Science and Engineering*, vol. 42, pp. 157–168, Jun. 2017, doi: 10.1016/j.jngse.2017.02.047.

[31] C. P. Ezeakacha, A. Rabbani, S. Salehi, and A. Ghalambor, "Integrated Image Processing and Computational Techniques to Characterize Formation Damage," presented at the SPE International Conference and Exhibition on Formation Damage Control, Feb. 2018. doi: 10.2118/189509-MS.

[32] S. Cheng *et al.*, "Effect of Temperature on the Structure and Filtration Performance of Polypropylene Melt-Blown Nonwovens," *Autex Research Journal*, vol. 21, no. 2, pp. 207–217, 2021, doi: 10.2478/aut-2019-0067.

[33] H. Zhang *et al.*, "Design of Polypropylene Electret Melt Blown Nonwovens with Superior Filtration Efficiency Stability through Thermally Stimulated Charging," *Polymers*, vol. 12, no. 10, 2020, doi: 10.3390/polym12102341.

[34] S. Palchoudhury, M. Baalousha, and J. R. Lead, "Chapter 5 - Methods for Measuring Concentration (Mass, Surface Area and Number) of Nanomaterials," in *Frontiers of Nanoscience*, vol. 8, M. Baalousha and J. R. Lead, Eds. Elsevier, 2015, pp. 153–181. doi: 10.1016/B978-0-08-099948-7.00005-1.

[35] S. Fu *et al.*, “Accurate characterization of full pore size distribution of tight sandstones by low-temperature nitrogen gas adsorption and high-pressure mercury intrusion combination method,” *Energy Science & Engineering*, vol. 9, no. 1, pp. 80–100, Jan. 2021, doi: 10.1002/ese3.817.

[36] P. Gill, T. T. Moghadam, and B. Ranjbar, “Differential scanning calorimetry techniques: applications in biology and nanoscience,” *J Biomol Tech*, vol. 21, no. 4, pp. 167–193, Dec. 2010.

[37] A. Oberlintner, M. Bajić, G. Kalčíková, B. Likozar, and U. Novak, “Biodegradability study of active chitosan biopolymer films enriched with Quercus polyphenol extract in different soil types,” *Environmental Technology & Innovation*, vol. 21, p. 101318, Feb. 2021, doi: 10.1016/j.eti.2020.101318.

[38] M. S. Thomas *et al.*, “Electrospun polylactic acid-chitosan composite: a bio-based alternative for inorganic composites for advanced application,” *Journal of Materials Science: Materials in Medicine*, vol. 29, no. 9, p. 137, Aug. 2018, doi: 10.1007/s10856-018-6146-1.

[39] H. Rosenheim, I. De, and S. Hyvedemm, “EN 13432 CERTIFIED BIOPLASTICS,” Apr. 2015. [Online]. Available: https://docs.european-bioplastics.org/publications/bp/EUBP_BP_En_13432.pdf

[40] “Product Data Sheet Luminy® L105.” Total Corbion, Jan. 12, 2021. Accessed: Oct. 10, 2020. [Online]. Available: https://www.total-corbion.com/media/skbpolcb/pds-luminy-l105-210112.pdf

[41] J. Bonilla and P. J. A. Sobral, “Disintegrability under composting conditions of films based on gelatin, chitosan and/or sodium caseinate containing boldo-of-Chile leafs extract,” *International Journal of Biological Macromolecules*, vol. 151, pp. 178–185, May 2020, doi: 10.1016/j.ijbiomac.2020.02.051.

[42] C. Vasile *et al.*, “Study of the soil burial degradation of some PLA/CS biocomposites,” *Composites Part B: Engineering*, vol. 142, pp. 251–262, Jun. 2018, doi: 10.1016/j.compositesb.2018.01.026.

[43] W. J. Sichina, “DSC as Problem Solving Tool: Measurement of Percent Crystallinity of Thermoplastics,” *Thermal Analysis*, p. 4.

[44] E. Dzierzkowska *et al.*, “Effects of Process Parameters on Structure and Properties of Melt-Blown Poly(Lactic Acid) Nonwovens for Skin Regeneration,” *Journal of Functional Biomaterials*, vol. 12, no. 1, 2021, doi: 10.3390/jfb12010016.

[45] Y. Xu, T. Wang, and X. Shi, “Enhanced dielectric and capacitive performance in polypropylene/poly(vinylidene fluoride) binary blends compatibilized with polydopamine,” *Materials & Design*, vol. 195, p. 109004, Oct. 2020, doi: 10.1016/j.matdes.2020.109004.

[46] S. N. Chirkov, “The Antiviral Activity of Chitosan (Review),” *Applied Biochemistry and Microbiology*, vol. 38, no. 1, pp. 1–8, Jan. 2002, doi: 10.1023/A:1013206517442.

[47] H. Li, Z. Wang, H. Zhang, and Z. Pan, “Nanoporous PLA/(Chitosan Nanoparticle) Composite Fibrous Membranes with Excellent Air Filtration and Antibacterial Performance,” *Polymers (Basel)*, vol. 10, no. 10, p. 1085, Sep. 2018, doi: 10.3390/polym10101085.

[48] T. T. T. Nguyen, O. H. Chung, and J. S. Park, “Coaxial electrospun poly(lactic acid)/chitosan (core/shell) composite nanofibers and their antibacterial activity,” *Carbohydrate Polymers*, vol. 86, no. 4, pp. 1799–1806, Oct. 2011, doi: 10.1016/j.carbpol.2011.07.014.

[49] S. Liu, S. Qin, M. He, D. Zhou, Q. Qin, and H. Wang, “Current applications of poly(lactic acid) composites in tissue engineering and drug delivery,” *Composites Part B: Engineering*, vol. 199, p. 108238, Oct. 2020, doi: 10.1016/j.compositesb.2020.108238.

[50] S. F. Gomaa, T. M. Madkour, S. Moghannem, and I. M. El-Sherbiny, “New polylactic acid/ cellulose acetate-based antimicrobial interactive single dose nanofibrous wound dressing mats,” *International Journal of Biological Macromolecules*, vol. 105, pp. 1148–1160, Dec. 2017, doi: 10.1016/j.ijbiomac.2017.07.145.

ANNEXE – SYNOPSIS FRANCAIS

Développement d'un matériau de filtration antiviral et compostable pour masques chirurgicaux

1 INTRODUCTION

Lors de la pandémie COVID-19, les masques faciaux se sont avérés efficaces pour réduire la transmission de ce virus respiratoire. Ils resteront sûrement la première ligne de défense lors de la prochaine épidémie de maladie respiratoire. Avec plus de temps libre causé par l'arrêt de toutes activités sociales, il est devenu clair que l'ampleur de cette pandémie ainsi que notre relation avec la planète et ses ressources sont étroitement liées. Des études montrent que l'épuisement des habitats naturels a rapproché les humains plus que jamais aux animaux porteurs d'agents pathogènes. Ainsi, certains prédisent que l'humanité verra une augmentation de la transmission des maladies des animaux aux humains [1]. De plus, au milieu du chaos de la pandémie, les gens du monde entier ont connu des saisons record d'incendies de forêt, d'inondations et d'ouragans. Il est clair que la pandémie n'est pas le seul danger mortel auquel l'humanité est confrontée - le changement climatique et l'effondrement des écosystèmes ont et continueront d'introduire des menaces pour les humains.

Notre économie mondiale a actuellement une chaîne d'approvisionnement linéaire pour la plupart des produits que nous utilisons ; les matières premières sont extraites du sol, transformées en un produit, qui est ensuite consommé et finalement jeté dans une décharge. En 2020, 52 milliards de masques en plastique ont été produits ; la matière première pour ceux-ci étant le pétrole [2]. Ces masques, qui sont rarement recyclés, ont presque tous fini dans les décharges [3]. Pour résoudre les problèmes d'épuisement des ressources et de transmission de ce virus mortel, l'idée est née de développer un produit qui peut aider à résoudre les deux ; améliorer notre capacité à lutter contre la pandémie tout en diminuant les déchets qu'on produit. Ce travail traite discute le développement d'un masque facial antiviral et compostable qui peut non seulement protéger l'humanité contre les maladies aéroportées, mais le fait tout en mettant en œuvre les principes d'une

économie circulaire. Les humains ne devraient plus prendre de la terre uniquement pour jeter ses ressources dans une décharge ; au contraire, nous devrions retourner les ressources de la Terre au sol et réutiliser ces ressources indéfiniment.

1.1 Masques

Les masques faciaux sont une partie intégrale de la stratégie mondiale pour l'atténuation de la pandémie de COVID-19. Les maladies respiratoires, telles que COVID-19, peuvent se propager dans l'air lorsque les personnes infectées respirent ou parlent, libérant des aérosols contenant des virus dans l'air qui sont ensuite inhalés par d'autres personnes à proximité. Les masques agissent donc comme la première barrière entre une personne infectée et le monde extérieur, tout en protégeant également les personnes non infectées de l'inhalation du virus. Les masques chirurgicaux sont généralement constitués de trois couches de tissu en polypropylène (PP). La couche centrale est faite d'un matériau de filtration, généralement fabriqué par extrusion soufflage pour produire des microfibres. Cette couche est le sujet de cette thèse.

1.1.1 Spécifications du masque chirurgical

Parce que ce travail vise à développer un masque pouvant remplacer les masques chirurgicaux en polypropylène qui sont déjà sur le marché, il est essentiel que le masque réponde à certaines spécifications pour les masques chirurgicaux. Afin de répondre aux exigences, le masque chirurgical doit posséder certaines propriétés. Premièrement, il doit être suffisamment poreux pour permettre à l'air de circuler confortablement à travers le filtre. Cependant, ces fibres doivent être suffisamment tassées afin d'empêcher le passage des molécules à travers le filtre. Afin de maximiser la filtration, il est important que le filtre retienne une charge électrostatique. De plus, le filtre doit être hydrophobe pour empêcher la pénétration d'aérosols à travers le filtre, car cela pourrait contribuer à la pénétration de particules pathogènes à travers le masque. De plus, l'hydrophobie de la surface du filtre peut empêcher l'adhésion microbienne, améliorant ainsi la protection de l'utilisateur [5]. Des exigences supplémentaires pour le filtre développé ici incluent la compostabilité du filtre ainsi que l'activité antivirale de la surface.

1.2 **Mécanisme antiviral**

Le virus SARS-CoV-2 est un coronavirus enveloppé, ce qui signifie que son ARN est contenu dans une membrane lipidique, similaire à celle qui enveloppe les cellules vivantes. Il a un diamètre extérieur de 91 ± 11 nm, mesuré autour de la circonférence des protéines qui forment sa « couronne » caractéristique. Ces pointes sont chargées positivement le long du sommet de la protéine, ce qui permet au virus de se lier et d'infecter les cellules hôtes [6] [7]. Les glycoprotéines de pointe, cependant, ne sont pas uniformément chargées; ils ont une charge nette négative sur les parties médiane et inférieure de la pointe [8]. La membrane lipidique du virus est également positive [9].

Les virus infectent les cellules hôtes en s'attachant à leur membrane, puis en insérant leur ARN dans la cellule vivante. Ils utilisent ensuite les mécanismes de réplication de la cellule pour répliquer l'ARN viral. Cependant, lorsque la membrane du virus est brisée, son ARN s'échappe du virus, le rendant inactif [10]. En général, on pense que les polycations adhèrent aux membranes des bicouches lipidiques et induisent une ségrégation ou une migration transmembranaire des molécules lipidiques, entraînant une fuite de l'ARN viral [11]. C'est le mécanisme ciblé pour l'activité antivirale ; il se résume dans Figure 1 ci-dessous [12].

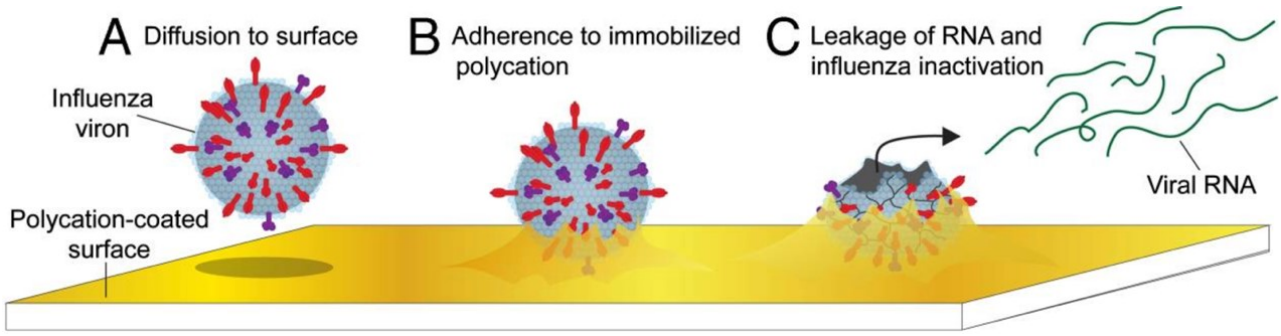

Figure 1. Mécanisme antiviral proposé : une rupture de la membrane et une fuite d'ARN [12].

Hsu et al. ont précédemment démontré le comportement antiviral de polymères cationiques contre le virus de la grippe. Comme le SARS-CoV-2 et les bactéries pathogènes, le virus de la grippe est également enveloppé d'une membrane lipidique [13]. Dans ses travaux, le N,N - Dodécyl,méthyl-polyéthylèneimine (PEI), un polymère

polycationique, démontre une réduction de 10 000 fois de l'infectivité virale en quelques minutes de contact avec le virus de la grippe [10].

D'autres polymères polycationiques ont été étudiés pour évaluer leur activité antivirale. Dans ce travail, le chitosane, un biopolymère antimicrobien connu, est étudié. Des études ont été entreprises pour évaluer l'effet antibactérien de la charge cationique du chitosane. Par la même logique utilisée par Hsu et. al, les propriétés antibactériennes du chitosane peuvent se traduire par des propriétés antivirales dans les virus enveloppés.

1.3 Matériaux

Le chitosane est un biopolymère dérivé de la désacétylation de la chitine, qui peut être facilement obtenu à partir des carapaces de crustacés. Sa structure est visible dans Figure 2. A un pH inférieur à 6,5, les groupements amines s'ionisent, conférant une charge cationique au polymère ainsi que lui permettant de se dissoudre en milieu acide.

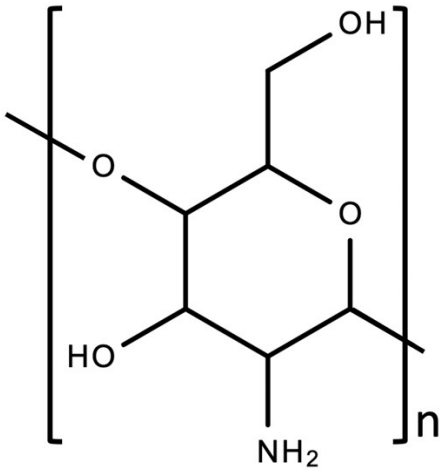

Figure 2. Structure moléculaire du chitosane.

Le mécanisme proposé ici repose sur la charge cationique du chitosane pour inactiver le virus. Étant donné que les molécules d'eau dans l'air expiré ont un pH légèrement acide, les gouttelettes d'aérosol exhalées par un individu infecté peuvent entraîner l'ionisation

locale des molécules de chitosane sur le masque [15]. Les groupements aminés chargés peuvent alors entrer en contact avec des virus en suspension dans cette gouttelette, interférant ainsi avec leur enveloppe et les rendant inactifs. Il a été suggéré qu'un chitosane de poids moléculaire plus élevé aurait un effet antiviral plus important en raison de la longue longueur de chaîne, qui pourrait pénétrer entre les pointes à la surface d'un coronavirus, interagissant directement avec la membrane d'enveloppe [16] [17].

Le poly(acide lactique) (PLA) est utilisé dans ce travail pour former les fibres non tissées. Ce polyester thermoplastique peut être dérivé de matières végétales, telles que le maïs ou la canne à sucre, ce qui en fait un polymère renouvelable [18]. Le PLA a des propriétés mécaniques similaires à celles du PP, ce qui en fait un substitut biodégradable approprié dans les masques faciaux. De plus, comme le PP, il s'agit d'un matériau électret et peut donc retenir une charge électrostatique [19]. Le PLA est notamment le biopolymère le plus largement utilisé et le moins cher du marché et peut être obtenu relativement facilement. Ainsi, du point de vue de la commercialisation, il s'agit d'un polymère idéal car il est déjà disponible à un coût similaire à celui du polypropylène.

1.4 Objectifs et contributions de la thèse

Les objectifs de ce travail sont les suivants :

1) Produire des fibres PLA via la méthode de pyrolyse par pulvérisation, appliquer une couche de chitosane et caractériser la morphologie et la structure des fibres.

2) Évaluer les performances de filtration des fibres en tant que matériau de filtration.

3) Étudier la compostabilité du filtre de manière efficace dans le temps.

4) Étudier les propriétés antivirales conférées par la couche de chitosane contre HCoV-OC43, le virus responsable de la grippe.

2 MÉTHODES

2.1 Préparation du filtre PLA

Le PLA a été dissous dans du dichlorométhane pour crée une solution de 8% PLA en poids. La solution a ensuite été pulvérisée à l'aide d'un aérographe obtenu auprès de Badger Air-Brush Co (Franklin Park, IL, USA) à 25 cm de la surface d'un bain d'eau à température ambiante en utilisant une pression de 0,2 MPa. Par le temps que la solution de polymère arrive à la surface de l'eau, le solvant se vaporise, laissant derrière lui des microfibres de PLA. La configuration du processus de pyrolyse par pulvérisation est illustrée dans Figure 3.

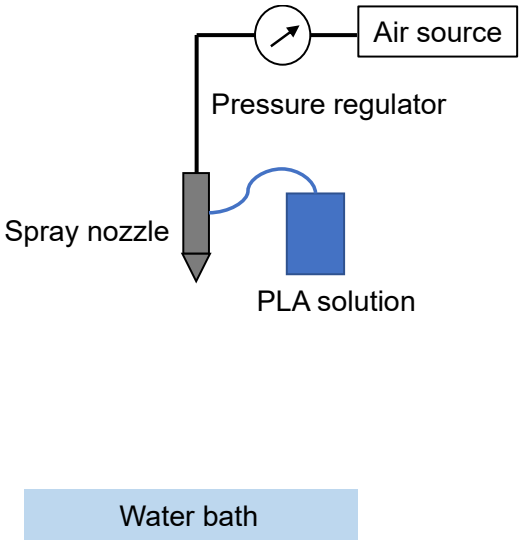

Figure 3. Configuration pour la production de filtres PLA par pyrolyse par pulvérisation.

3 RÉSULTATS EXPÉRIMENTAUX

3.1 Filtration et différentiel de pression

La filtration des aérosols des filtres chirurgicaux, PLA, PLA/CS1 et PLA/CS 2 est illustrée dans Tableau 1. Tous les filtres ont des niveaux de filtration similaires à ceux du filtre du masque chirurgical, à environ 98 %. Le différentiel de pression avec les aérosols pour les filtres PLA, PLA/CS1 et PLA/CS 2 est plus élevé que pour le filtre chirurgical. Cependant,

sans aérosols, cette différence est négligeable. Un différentiel de pression plus faible est souhaité afin d'obtenir un filtre plus confortable pour l'utilisateur.

Tableau 1. Filtration moyenne et différentiel de pression avec provocation aérosol avec intervalle de confiance à 95% pour les filtres testés.

Matériel	Filtrage moyen (%)	Différentiel de pression avec les aérosols (Pa)	Différentiel de pression sans aérosols (Pa)
Chirurgical	97,67 ± 1,1	126 ± 23	15,4 ± 0,5
PLA	97,93 ± 1,6	164 ± 38	11,5 ± 2,1
PLA/CS1	97,90 ± 1,8	196 ± 53	11,4 ± 5,4
PLA/CS2	97,57 ± 2,0	250 ± 75	14,4 ± 4,1

Il existe un grand intervalle de confiance pour les échantillons PLA, PLA/CS 1 et PLA/CS2 en raison de la variabilité induite lors de la production de filtres. Le filtre chirurgical est produit commercialement et a une distribution de fibre uniforme, et a donc un différentiel de pression plus uniforme d'un filtre à l'autre.

3.2 **Angle de contact**

Figure 4 ci-dessous résume les mesures d'angle de contact effectuées pour les filtres PLA, PLA/CS1 et PLA/CS2 par rapport à la couche de filtration de masque chirurgical. Tous les filtres sont hydrophobes, ce qui est important pour minimiser la pénétration des aérosols à travers le masque. La couche de filtration du filtre chirurgical, le filtre PLA et le filtre PLA/CS1 n'ont pas d'angles de contact statistiquement significatifs au niveau p=0,05. Cependant, PLA/CS2 démontre une diminution statistiquement significative de l'angle de contact par rapport aux filtres, indiquant que la surface a une mouillabilité légèrement plus élevée. Cette augmentation de la mouillabilité est probablement due à la propriété hydrophile du chitosane, ainsi qu'à la formation de films entre les fibres de PLA. Ces films diminuent l'effet de la microstructure des fibres sur l'énergie de surface du filtre. Ainsi, les aérosols déposés à la surface du filtre vont imprégner le filtre PLA/CS2 plus rapidement que les filtres avec moins de

chitosane. Malgré cela, les échantillons de PLA/CS2 présentent des propriétés de surface relativement hydrophobes.

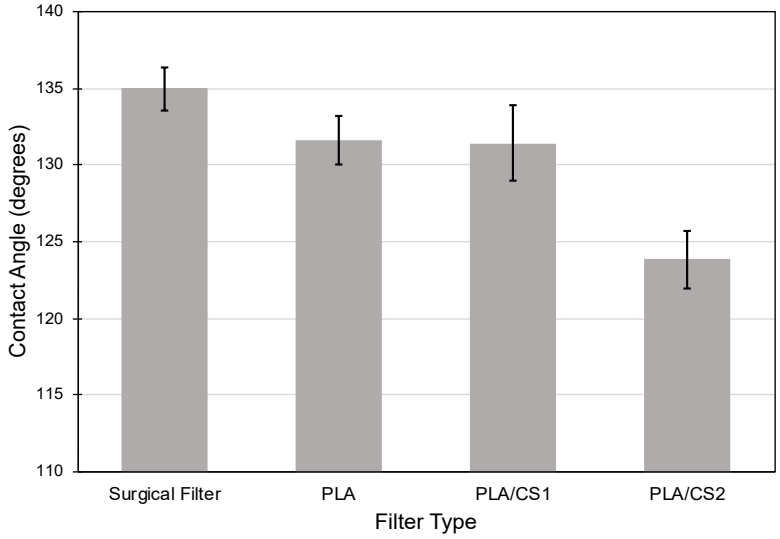

Figure 4. **Mesures d'angle de contact pour les filtres testés. Les barres d'erreur désignent l'intervalle de confiance à 95 %. Remarque : l'axe des y commence à 110° pour mieux démontrer les différences entre les échantillons.**

3.3 **Morphologie des fibres**

Afin de produire des fibres d'une manière rapide et facile, la pyrolyse par pulvérisation de la solution de polymère a été utilisée au lieu de la méthode typique d'extrusion soufflage, qui nécessite un équipement coûteux. Figure 5 ci-dessous montre les différences dans la morphologie des fibres PLA faites par la pyrolyse par rapport aux fibres PP faites par extrusion soufflage. Notamment, les fibres soufflées sont plus régulières et linéaires comparées aux fibres faites par pyrolyse. En outre, les fibres soufflées sont uniformément réparties, tandis que les fibres pyrolysées ont tendance à s'agglomérer en faisceaux. Ainsi, dans le procédé de coulée au solvant de production de fibres polymères, deux diamètres de fibres peuvent être caractérisés : les diamètres des fibres individuelles, ainsi que les diamètres des faisceaux de fibres.

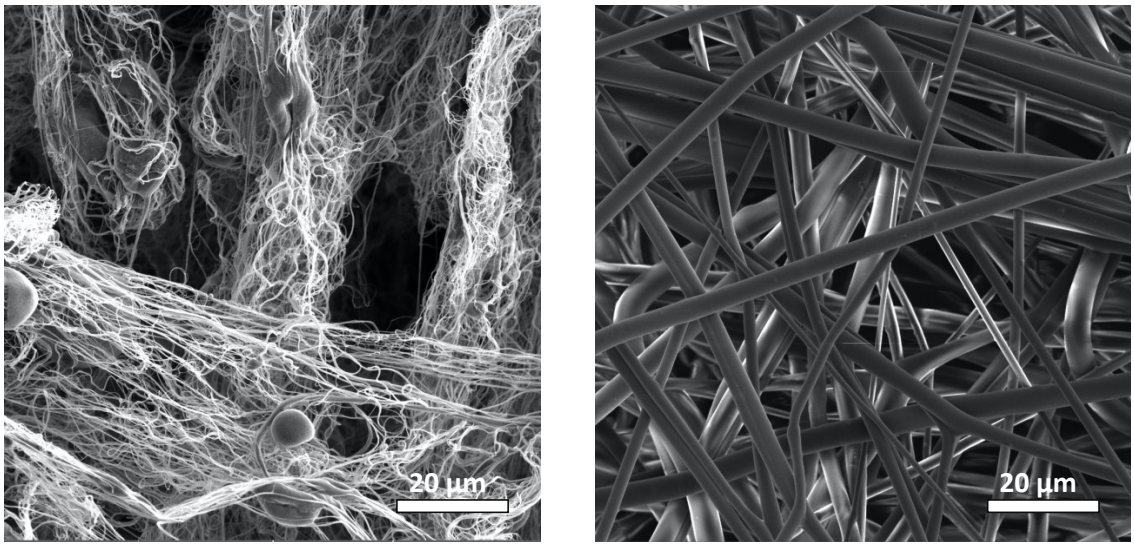

Figure 5. **Images MEB de fibres PLA pyrolysées (à gauche) et de fibres PP soufflées (à droite).**

Figure 6 ci-dessous montre la morphologie du filtre des fibres de PLA après l'application du chitosane. Plutôt que de couvrir chaque fibre PLA individuellement, le chitosane forme un film entre certaines fibres. La concentration de la solution de chitosane utilisée est suffisamment faible pour qu'elle ne bloque pas complètement tout l'espace entre les fibres, permettant ainsi à l'air de passer.

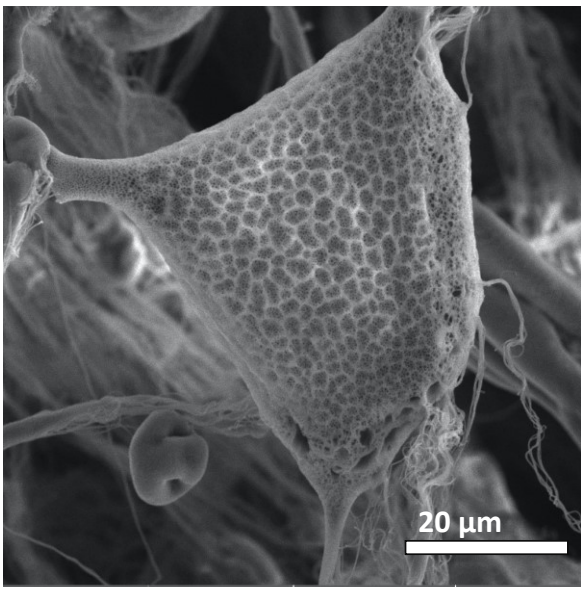

Figure 6. **Fibres PLA pyrolysées couvertes de chitosane.**

Les diamètres des fibres individuelles ont ensuite été calculés à l'aide de MATLAB. Comme représenté sur la Figure 7 ci-dessous, les fibres du masque chirurgical ont un plus large diamètre que celles des trois filtres préparés dans ce travail. Cela est probablement dû à la différence dans les méthodes de production; le filtre chirurgical est préparé par extrusion soufflage industriel, tandis que les trois autres sont préparés par pyrolyse à pulvérisation à l'échelle du laboratoire. Il n'y a pas de différence statistiquement significative entre les diamètres des trois filtres préparés par pyrolyse. Cela confirme que le chitosane ne recouvre pas les fibres de PLA individuelles, mais forme plutôt des films intermittents entre certaines fibres dans le filtre.

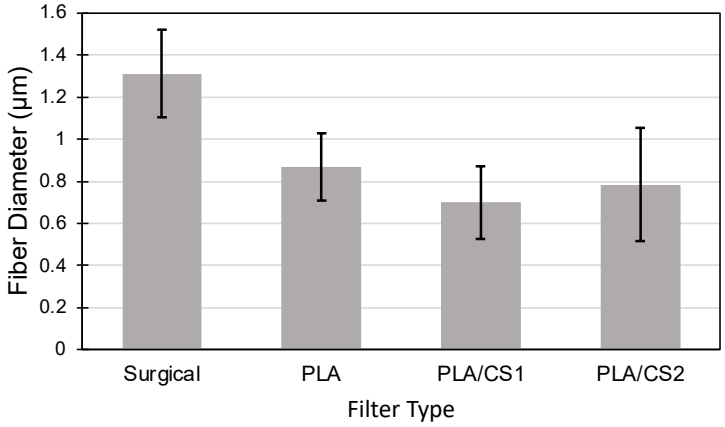

Figure 7. **Diamètres de fibre pour différents types de filtres mesurés à partir d'images MEB à l'aide de MATLAB. Les barres d'erreurs montrent les déviations standards.**

3.4 **Cristallinité**

EN-13432 est la norme en vigueur en Europe pour les bioplastiques compostables et est reconnue dans le monde entier. Selon cette norme, un plastique est considéré comme compostable s'il atteint une diminution de masse de 90 % après 3 mois [20]. Grade total Corbion L105 de PLA est certifié compostable selon la norme EN - 13432 jusqu'à une épaisseur de 2,3 mm [21]. Comme vérification préalable de la compostabilité des filtres, la cristallinité des fibres projetées est évaluée par calorimètre à analyse différentielle (DSC). Le but de cette étude est de vérifier que le traitement de nos fibres n'augmente pas la cristallinité du matériau par rapport aux pastilles de PLA telles que reçues, car cela

diminuerait probablement le taux de dégradation. Ainsi, si le taux de dégradation diminue, il est possible que le produit final ne réponde pas aux exigences de compostabilité selon EN-13432.

Ce rapport évalue uniquement la cristallinité et la dégradation du composant PLA du filtre puisque le chitosane a un taux de dégradation plus rapide que le PLA, se dégradant en quelques jours [22][23]. De plus, le chitosane étant un polymère hydrophile, son incorporation dans le filtre permet de puiser de l'eau accélérant ainsi l'hydrolyse du PLA [24]. Ainsi, la dégradation du PLA est le facteur limitant la vitesse.

Les températures de transition du polymère, indiquées dans Tableau 2, peuvent donner un aperçu de la cristallinité à température ambiante des fibres et des pastilles. Les fibres pulvérisées présentent des températures de transition vitreuse et de fusion inférieures à celles de la forme en pastilles, suggérant une structure plus amorphe. Ceci est probablement dû à la précipitation rapide du polymère due à l'évaporation du solvant, qui donne une structure plus amorphe que le polymère tel que reçu. Une précipitation rapide entraîne un volume libre plus important dans le matériau, ce qui explique la présence d'un pic de cristallisation immédiatement après la transition vitreuse de l'échantillon de fibre ; ce pic de cristallisation ne s'est pas produit dans l'échantillon de pastille puisque les chaînes polymères étaient déjà dans une structure organisée et stable.

Tableau 2. Températures de transition pour les granules et les fibres.

	T_g (° C)	T_m (° C)
Granules PLA	69,62	169,32
Fibres PLA	62,61	165,84

Les résultats suggèrent que les fibres sont plus amorphes à des températures inférieures à la transition vitreuse par rapport aux pastilles telles que reçues. Ceci est favorable à la dégradation dans des conditions de compost car la teneur en volume libre plus élevée permet une plus grande pénétration d'humidité, ce qui entraîne des taux d'hydrolyse plus

élevés. On peut donc supposer que les fibres ne mettront pas plus de temps à se dégrader par rapport au polymère d'origine certifié par la norme EN-13432.

3.5 **Rétention de charge électrostatique**

Figure 8 ci-dessous démontre que les masques PLA et PLA/CS ont une meilleure rétention de charge que le masque chirurgical PP sur une période de 4 heures. Le chitosane ne semble pas avoir d'impact significatif sur la rétention de charge du filtre.

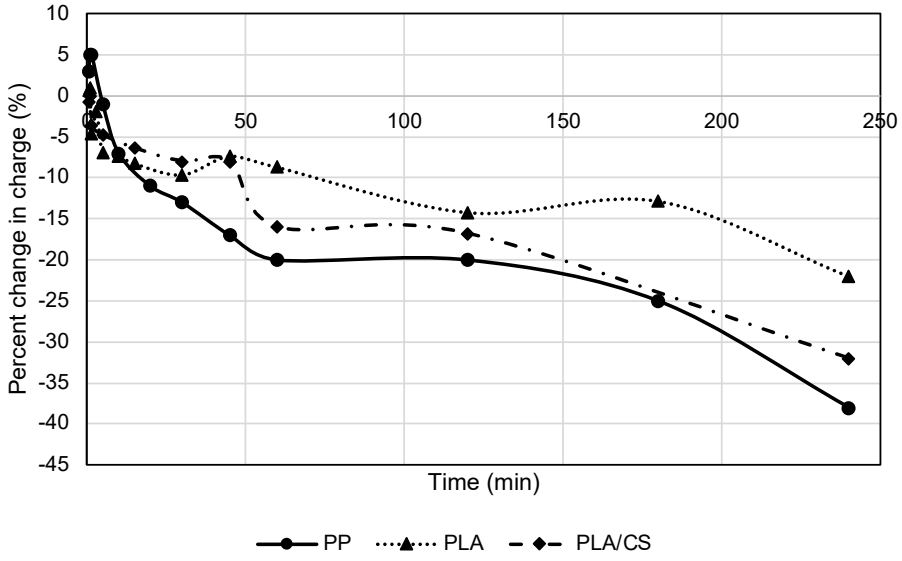

Figure 8. **Diminution de la charge électrostatique des échantillons de PP, PLA et PLA/CS1 sur une période isotherme de quatre heures.**

Les différences de rétention de charge entre les masques PLA et PP pourraient être attribuées à des différences de cristallinité des polymères. Étant donné que les charges sont piégées par les cristallites dans le polymère, un polymère plus cristallin aura une rétention de charge plus importante qu'un polymère plus amorphe. Bien que la cristallinité de ce masque PP spécifique n'ait pas été quantifiée dans ce travail, d'autres recherches ont démontré que la cristallinité des masques chirurgicaux en PP est relativement faible, à environ 21 % à 20 °C [25]. Les fibres de PLA préparées dans ce travail, cependant, ont un degré de cristallinité de 59,5%, comme cela a été calculé à partir des données DSC. Il est donc possible que la concentration et la rétention de charge plus élevées des filtres PLA soient attribuées à une cristallinité plus élevée.

3.6 **Propriété antivirale**

Les résultats du premier essai du test antiviral sont présentés dans Figure 9. Il n'y a pas de différence statistiquement importante entre les échantillons de référence, de contrôle (PLA) et PLA/CS1. Cependant, l'échantillon PLA/CS2, avec une concentration élevée en chitosane, démontre une réduction de 0,83 fois de l'infectivité par rapport à l'échantillon de référence sans textile. Cela représente une réduction de 0,61 fois par rapport à l'échantillon témoin PLA. Ces résultats ne correspondent pas à des propriétés antivirales significatives; typiquement, une diminution de l'infectivité d'au moins 10 fois est nécessaire pour considérer un matériau comme étant antiviral. Ainsi, les résultats de cette expérience ne démontrent pas de comportement antiviral.

L'expérience a été répétée avec une concentration de virus plus diluée. Le raisonnement derrière ce changement est qu'il peut y avoir eu un nombre trop élevé de virus en contact avec l'échantillon par rapport au nombre de sites chargés sur le chitosane. Les résultats de cet essai sont présentés dans Figure 9. Ces données ne sont pas concluantes car les échantillons contenant du chitosane avaient un nombre plus élevé de virus actifs par rapport à l'échantillon PLA. Comme mentionné précédemment, les valeurs enregistrées sont relativement similaires pour tous les échantillons ; pas assez de réduction de l'infectivité virale n'a été enregistrée pour tirer des conclusions de ce test.

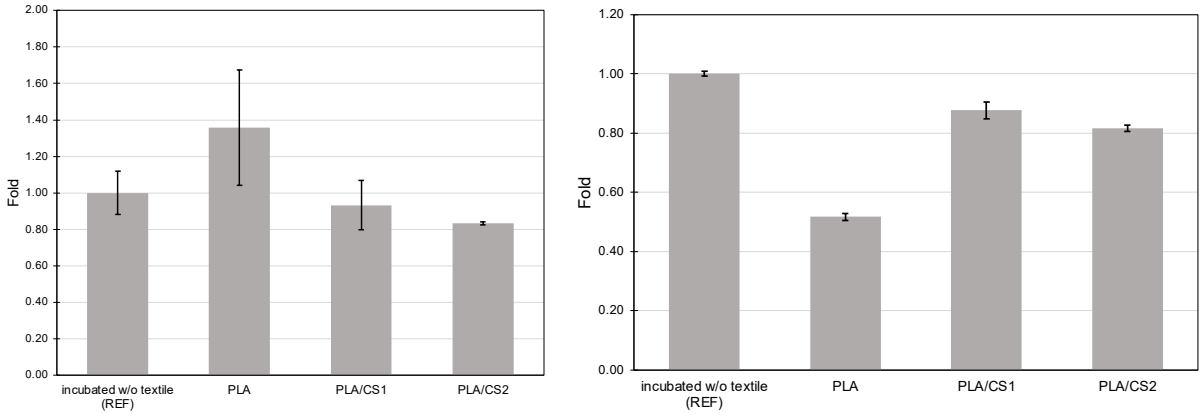

Figure 9. **Premier essai de dosage antiviral avec HCoV-OC43 (à gauche) et deuxième essai utilisant une solution plus diluée (à droite).**

4 CONCLUSION

Dans ce travail, un matériau de filtration compostable est produit utilisant un procédé peu coûteux et accessible. Les tests préliminaires révèlent que ce matériau en fibres non tissées fonctionne de manière similaire à la couche filtrante typique du masque chirurgical en polypropylène en ce qui concerne la filtration et la résistance au passage d'air. De plus, il a été démontré que ce processus de pyrolyse par pulvérisation produit des fibres plus petites que les fibres soufflées du masque chirurgical. Ce processus a entraîné une légère diminution de la cristallinité par rapport au PLA brut, ce qui pourrait potentiellement contribuer un temps de dégradation plus rapide. Des régions cristallines suffisantes restent dans les fibres pour qu'elles puissent retenir la charge ; ceci, combiné aux propriétés d'électret du PLA, donne un masque qui peut mieux retenir la charge que le masque chirurgical en polypropylène. Une couche de chitosane a été ajouté qui n'a pas eu d'impact significatif sur l'hydrophobie de la surface globale. L'activité antivirale de cette couche de chitosane a été testée contre HCoV-OC43, mais l'expérience n'a pas été concluante.

RÉFÉRENCES – SYNOPSIS FRANÇAIS

[1] H. F. Lorentzen, T. Benfield, S. Stisen, and C. Rahbek, “COVID-19 is possibly a consequence of the anthropogenic biodiversity crisis and climate changes,” p. 6.

[2] “Medical Face Mask Market - Global Outlook and Forecast 2020-2025,” Arizton Advisory and Intelligence, Jun. 2020. Accessed: Apr. 10, 2021. [Online]. Available: https://www.marketresearch.com/Arizton-v4150/Medical-Face-Mask-Global-Outlook-13345767/

[3] N. B. Rodríguez, G. Formentini, C. Favi, and M. Marconi, “Environmental implication of personal protection equipment in the pandemic era: LCA comparison of face masks typologies,” *Procedia CIRP*, vol. 98, pp. 306–311, Jan. 2021, doi: 10.1016/j.procir.2021.01.108.

[4] “Effectiveness of Masks: Fast Answers with Automated SEM Analysis,” *Nanoscience Instruments*. https://www.nanoscience.com/applications/materials-science/effectiveness-of-masks-fast-answers-with-automated-sem-analysis/ (accessed Oct. 11, 2021).

[5] F23 Committee, “Specification for Performance of Materials Used in Medical Face Masks,” ASTM International. doi: 10.1520/F2100-19.

[6] Z. Adamczyk, P. Batys, and J. Barbasz, “SARS-CoV-2 virion physicochemical characteristics pertinent to abiotic substrate attachment,” *Current Opinion in Colloid & Interface Science*, vol. 55, p. 101466, Oct. 2021, doi: 10.1016/j.cocis.2021.101466.

[7] X. Ou *et al.*, “Characterization of spike glycoprotein of SARS-CoV-2 on virus entry and its immune cross-reactivity with SARS-CoV,” *Nature Communications*, vol. 11, no. 1, p. 1620, Mar. 2020, doi: 10.1038/s41467-020-15562-9.

[8] Turoňová Beata *et al.*, “In situ structural analysis of SARS-CoV-2 spike reveals flexibility mediated by three hinges,” *Science*, vol. 370, no. 6513, pp. 203–208, Oct. 2020, doi: 10.1126/science.abd5223.

[9] P. H. Pawłowski, “Charged amino acids may promote coronavirus SARS-CoV-2 fusion with the host cell,” *AIMSBPOA*, vol. 8, no. 1, Art. no. biophy-08-01-008, 2021, doi: 10.3934/biophy.2021008.

[10] J. Haldar, D. An, L. Álvarez de Cienfuegos, J. Chen, and A. M. Klibanov, “Polymeric coatings that inactivate both influenza virus and pathogenic bacteria,” *Proc Natl Acad Sci USA*, vol. 103, no. 47, p. 17667, Nov. 2006, doi: 10.1073/pnas.0608803103.

[11] V. A. Kabanov and A. A. Yaroslavov, “What happens to negatively charged lipid vesicles upon interacting with polycation species?,” *Journal of Controlled Release*, vol. 78, no. 1, pp. 267–271, Jan. 2002, doi: 10.1016/S0168-3659(01)00496-5.

[12] B. B. Hsu, S. Y. Wong, P. T. Hammond, J. Chen, and A. M. Klibanov, “Mechanism of inactivation of influenza viruses by immobilized hydrophobic polycations,” *Proceedings of the National Academy of Sciences*, vol. 108, pp. 61–66, 2010.

[13] V. S. Mandala, M. J. McKay, A. A. Shcherbakov, A. J. Dregni, A. Kolocouris, and M. Hong, “Structure and drug binding of the SARS-CoV-2 envelope protein transmembrane domain in lipid bilayers,” *Nature Structural & Molecular Biology*, vol. 27, no. 12, pp. 1202–1208, Dec. 2020, doi: 10.1038/s41594-020-00536-8.

[14] F. Sami El-banna, M. E. Mahfouz, S. Leporatti, M. El-Kemary, and N. A. N. Hanafy, “Chitosan as a Natural Copolymer with Unique Properties for the Development of Hydrogels,” *Applied Sciences*, vol. 9, no. 11, 2019, doi: 10.3390/app9112193.

[15] T. Kullmann, I. Barta, B. Antus, M. Valyon, and I. Horváth, “Environmental temperature and relative humidity influence exhaled breath condensate pH,” *Eur Respir J*, vol. 31, no. 2, p. 474, Feb. 2008, doi: 10.1183/09031936.00128007.

[16] S. N. Kulikov, S. N. Chirkov, A. V. Il’ina, S. A. Lopatin, and V. P. Varlamov, “Effect of the molecular weight of chitosan on its antiviral activity in plants,” *Applied Biochemistry and Microbiology*, vol. 42, no. 2, pp. 200–203, Mar. 2006, doi: 10.1134/S0003683806020165.

[17] V. N. Davydova *et al.*, “Chitosan antiviral activity: Dependence on structure and depolymerization method,” *Applied Biochemistry and Microbiology*, vol. 47, no. 1, pp. 103–108, Jan. 2011, doi: 10.1134/S0003683811010042.

[18] L. W. McKeen, “13 - Environmentally Friendly Polymers,” in *Permeability Properties of Plastics and Elastomers (Third Edition)*, L. W. McKeen, Ed. Oxford: William Andrew Publishing, 2012, pp. 287–304. doi: 10.1016/B978-1-4377-3469-0.10013-X.

[19] J. Zhang, G. Chen, G. S. Bhat, H. Azari, and H. Pen, “Electret characteristics of melt-blown polylactic acid fabrics for air filtration application,” *Journal of Applied Polymer Science*, vol. 137, no. 4, p. 48309, Jan. 2020, doi: 10.1002/app.48309.

[20] A. Oberlintner, M. Bajić, G. Kalčíková, B. Likozar, and U. Novak, “Biodegradability study of active chitosan biopolymer films enriched with Quercus polyphenol extract in different soil types,” *Environmental Technology & Innovation*, vol. 21, p. 101318, Feb. 2021, doi: 10.1016/j.eti.2020.101318.

[21] M. S. Thomas *et al.*, “Electrospun polylactic acid-chitosan composite: a bio-based alternative for inorganic composites for advanced application,” *Journal of Materials Science: Materials in Medicine*, vol. 29, no. 9, p. 137, Aug. 2018, doi: 10.1007/s10856-018-6146-1.

[22] H. Zhang *et al.*, “Design of Polypropylene Electret Melt Blown Nonwovens with Superior Filtration Efficiency Stability through Thermally Stimulated Charging,” *Polymers*, vol. 12, no. 10, 2020, doi: 10.3390/polym12102341.

[23] H. Rosenheim, I. De, and S. Hyvedemm, “EN 13432 CERTIFIED BIOPLASTICS,” Apr. 2015. [Online]. Available: https://docs.european-bioplastics.org/publications/bp/EUBP_BP_En_13432.pdf

[24] “Product Data Sheet Luminy® L105.” Total Corbion, Jan. 12, 2021. Accessed: Oct. 10, 2020. [Online]. Available: https://www.total-corbion.com/media/skbpolcb/pds-luminy-l105-210112.pdf

[25] S. Cheng *et al.*, “Effect of Temperature on the Structure and Filtration Performance of Polypropylene Melt-Blown Nonwovens,” *Autex Research Journal*, vol. 21, no. 2, pp. 207–217, 2021, doi: 10.2478/aut-2019-0067.